PUBLICATIONS OF THE ASTRONOMICAL SOCIETY OF THE PACIFIC, **127**:102–125, 2015 February

Revised Filter Profiles and Zero Points for Broadband Photometry

ANDREW W. MANN[1,2] AND KASPAR VON BRAUN[3,4]

Received 2014 November 04; accepted 2014 December 05; published 2015 January 26

ABSTRACT. Estimating accurate bolometric fluxes for stars requires reliable photometry to absolutely flux calibrate the spectra. This is a significant problem for studies of very bright stars, which are generally saturated in modern photometric surveys. Instead we must rely on photometry with less precise calibration. We utilize precisely flux-calibrated spectra to derive improved filter bandpasses and zero points for the most common sources of photometry for bright stars. In total, we test 39 different filters in the General Catalog of Photometric Data as well as those from Tycho-2 and *Hipparcos*. We show that utilizing inaccurate filter profiles from the literature can create significant color terms resulting in fluxes that deviate by $\gtrsim$10% from actual values. To remedy this we employ an empirical approach; we iteratively adjust the literature filter profile and zero point, convolve it with catalog spectra, and compare to the corresponding flux from the photometry. We adopt the passband values that produce the best agreement between photometry and spectroscopy and are independent of stellar color. We find that while most zero points change by <5%, a few systems change by 10–15%. Our final profiles and zero points are similar to recent estimates from the literature. Based on determinations of systematic errors in our selected spectroscopic libraries, we estimate that most of our improved zero points are accurate to 0.5–1%.

Online material: color figures

1. INTRODUCTION

Stellar effective temperatures ($T_{\rm eff}$) are generally determined through a variety of indirect methods, such as the infrared flux method (IRFM, Blackwell & Shallis 1977; Casagrande et al. 2006, 2010), fitting observations to synthetic spectra (e.g., Valenti & Piskunov 1996), or using equivalent widths and/or line ratios (e.g., Sneden 1973; Sousa et al. 2010, 2011). Because of model errors and the need for a zero point for IRFM these methods must be calibrated using direct methods. The principal direct method is interferometry, which can be used to determine a star's angular diameter (θ). With θ and a measurement of the star's bolometric flux ($F_{\rm bol}$), we can calculate effective temperature from a rewritten form of the Stefan–Boltzmann Law:

$$T_{\rm eff} = \left(\frac{F_{\rm bol}}{\sigma(\theta/2)^2}\right)^{1/4}, \quad (1)$$

where σ is the Boltzmann constant. Because equation (1) defines $T_{\rm eff}$, it provides an empirical and accurate method to establish the true $T_{\rm eff}$ scale of stars.

Typically, $F_{\rm bol}$ is measured using flux-calibrated empirical templates (e.g., Pickles 1998) or models (Allard et al. 2012). Broadband photometry is used to inform which template or model is the best match to the star and used to derive the absolute flux calibration (for a more detailed description of this method see van Belle et al. 2008). Even when using the star's true spectrum instead of a template, the spectrum must be absolutely calibrated using photometry because of slit losses, atmospheric variability, etc. Thus both methods are sensitive to errors in photometry, particularly, errors common to entire photometric systems such as inaccuracies in the zero point and filter passband. Such errors could explain much of the systematic difference seen between $F_{\rm bol}$ values for the same stars when using different photometry (Boyajian et al. 2012; Mann et al. 2013b).

Most modern astronomical work can make use of precisely calibrated photometry from surveys such as the Sloan Digital Sky Survey (Stoughton et al. 2002; Abazajian et al. 2009) and the Two-Micron All-Sky Survey (2MASS, Skrutskie et al. 2006). However, long-baseline interferometry is currently limited to the largest and/or nearest stars, whose photometry is almost always saturated in such surveys. Instead, we must make use of older photometry, often from the General Catalog of Photometric Data (GCPD, Mermilliod et al. 1997),[5] which is a collection of photometry on $>200,000$ stars from >2500 papers. The GCPD contains more than 80 systems over a wide

[1] Harlan J. Smith Fellow, Department of Astronomy, The University of Texas at Austin, Austin, TX 78712.
[2] Visiting Researcher, Institute for Astrophysical Research, Boston University, Boston, MA 02215.
[3] Lowell Observatory, 1400 W. Mars Hill Rd., Flagstaff, AZ 86001.
[4] Max Planck Institute for Astronomy (MPIA), Konigstuhl 17, 69117 Heidelberg, Germany.

[5] Please see http://obswww.unige.ch/gcpd/.

range of wavelengths, which makes it particularly useful for flux calibrating spectra and deriving spectral-energy distributions for bright stars. However, most of these photometric systems are calibrated no more precisely than 5% (see Bohlin et al. [2014] and references within).

Recent improvements in reduction techniques and instrumentation for long-baseline optical interferometry (e.g., Ireland et al. 2008; ten Brummelaar et al. 2012) have enabled the measurement of the stellar angular diameters (θ) to better than 2% for stars of sufficient brightness and angular size (e.g., Berger et al. 2006; Boyajian et al. 2013; Huber et al. 2013; von Braun et al. 2014). Errors of 1–2% in the angular diameter result in errors in $T_{\rm eff}$ of just 0.5–1% ($\simeq$30 K for a Sun-like star) ignoring errors in $F_{\rm bol}$. In order to be limited by the error in θ (which is typically the harder quantity to measure) $F_{\rm bol}$ must be measured with an error $\lesssim$2%. More importantly, $F_{\rm bol}$ values need to be free of systematic errors, which could conceivably arise from zero point and filter profile errors in the photometry, deviations in the shape of the spectrum, or inaccurate corrections for interstellar reddening.

When converting magnitudes into fluxes, a slightly erroneous filter profile (i.e., different from the true system profile) or red leak will result in color-terms (Bessell 1990; Bessell & Brett 1988). Specifically, flux derived from convolving the filter profile with the spectrum will differ from the flux calculated from corresponding photometry as a function of the color of the star. One can reverse-engineer the filter passband by calculating synthetic fluxes from precisely calibrated spectra, then comparing these values to the corresponding flux derived from the photometry of the same stars (e.g., Straizys 1996; Maíz Apellániz 2006). The filter profile can be adjusted until the difference between the synthetic and observed fluxes is a constant independent of the star's color, and then the zero point adjusted until that constant is on average $\simeq$0. This method is entirely empirical, and takes into account the full system throughput, but is limited by systematic errors in the spectral flux calibration.

In this article, we make use of several well-calibrated spectroscopic libraries to verify and derive revised filter bandpasses, zero points, and corresponding errors for photometry of bright stars (GCPD, Tycho-2, and *Hipparcos*). In § 2, we describe our sample of spectroscopic libraries, and in § 3, we give a rundown of the photometric sample. In § 4, we explain how we derive new filter bandpasses by forcing the synthetic and observed photometry to give consistent fluxes. In § 5, we detail our revised properties for different photometric systems, compare our parameters to those in the literature, and estimate the error on our zero points. We conclude in § 6 with a brief summary and highlight how our findings can significantly alter conclusions about $F_{\rm bol}$ values for cool stars.

2. SPECTROSCOPIC SAMPLE

A spectroscopic sample that is optimal for our purposes would include a large number ($>$100) of stars with photometry in the GCPD covering a wide range in $B-V$ color, and contain spectra with significant wavelength coverage to include as many bands as possible. The MILES library (Sáchez-Bláquez et al. 2006; Falcón-Barroso et al. 2011) is one of the largest ($\simeq$1000 stars) and spans a wide range of $B-V$ colors. However, MILES spectra cover only 3525–7000 Å, which excludes sections of the bluest (e.g., Johnson U, Geneva U, Strömgren u) and reddest (e.g., Cousins I) optical filters. We resolve not to use MILES even for the passbands covered to maintain data homogeneity. Libraries like the Indo-U.S. Library (Valdes et al. 2004) have both wide wavelength coverage and a large number of stars, but the narrow slit, observing conditions, and joining of multiple observations with different gratings means that the flux calibration is unlikely to have sufficient precision and accuracy for our purposes.

For optical passbands, we use the Next Generation Spectral Library (NGSL, Gregg et al. 2006; Heap & Lindler 2007), which includes spectra of 374 stars spanning $-0.3 < B-V < 1.8$. NGSL spectra are taken with the Space Telescope Imaging Spectrograph (STIS) on the *Hubble Space Telescope* (*HST*) using three different gratings (G230LB, G430L, and G750L). This provides spectral coverage from 2000 Å to 10000 Å, which covers all filters we test. Although the NGSL library contains fewer stars than MILES, the superior wavelength coverage is critical because it enables us to include far more filter systems in our analysis. Further, the relative flux calibration of *HST* STIS spectra is expected to be accurate to 0.5% (Bohlin et al. 2001; Bohlin & Gilliland 2004a, b), which is superior to what can currently be achieved from the ground.

For the NIR bands (Johnson *JHKL*), we utilize the Infrared Telescope Facility (IRTF) spectral library (Cushing et al. 2005; Rayner et al. 2009), which includes 210 F, G, K, and M stars with wavelength coverage 8000–50,000 Å. Only $\simeq$ one third of these stars have *JHK* photometry in the GCPD, but this is better than comparable NIR catalogs, which tend to cover fainter stars that are less likely to be in the GCPD. The catalog also lacks the bluest stars ($B-V<0.15$), but goes significantly redder ($B-V>2$) than most spectroscopic catalogs.

Because only 49 stars in the IRTF library have NIR photometry in the GCPD, we supplement the IRTF spectra with NIR spectra from Mann et al. (2013a), Mann et al. (2013b), and Gaidos et al. (2014). All of these stars are K and M dwarfs, which biases the sample toward redder $B-V$ colors. However, the paucity of properly flux-calibrated NIR spectra makes this problem difficult to avoid. NIR spectra from these sources were taken with the same instrument and mode, and reduced in an identical manner to that of the IRTF library (Vacca et al. 2003; Cushing et al. 2004), except that the supplemental spectra cut off at 2.5 μm while most stars in the IRTF library extend to 5 μm.

We remove stars known to be highly variable ($\gtrsim$0.1 mag variability in V, Samus et al. 2004; Samus et al. 2010), stars lacking any photometry in the GCPD, those with an object of similar or greater brightness within 8″ (which will contaminate the photometry), and stars with questionable designations (e.g.,

the star labeled as GJ 15B in the NGSL catalog is probably GJ 15A based on the spectrum and *HST* pointing). This leaves 364 stars from the NGSL catalog, 49 stars from the IRTF library, and 59 stars from our supplemental spectra.

3. PHOTOMETRIC SYSTEMS

We focus our efforts on photometry from the GCPD because it is the most common source of photometry for bright interferometry stars. Many less commonly used systems in the GCPD,

TABLE 1
PHOTOMETRIC SYSTEMS AND INITIAL PARAMETERS

GCPD Name	Band	System reference(s)	Center (Å)	$W_{\rm eff}$[a] (Å)	$N_{\rm sp}$[b]	$N_{\rm ph}$[b]
UcBV,	Uc	Arp (1958)	3948	376	56	71
UBV,	U	Johnson & Morgan (1951),	3517	665	299	1708
UBVE	B	Bessell (1990)	4454	1037	314	2168
	V		5523	909	315	2373
	u		3466	339	273	817
uvby	b	Strömgren (1956),	4747	201	266	837
(Strömgren)	v	Crawford & Mander (1966)	4073	200	266	818
	y		5479	256	267	882
	U		3467	479	269	267
	B1		4030	424	269	267
	B		4266	806	269	267
Geneva	*B2*	Golay (1972)	4486	445	269	267
	V1		5417	508	269	267
	V		5524	779	269	267
	G		5821	485	269	267
	U		3450	395	180	387
	P		3740	276	180	387
	X		4054	254	181	392
Vilnius	Y	Kakaras et al. (1968)	4665	288	180	392
	Z		5162	232	180	392
	V		5442	294	180	392
	S		6534	212	179	377
	W		3546	453	171	171
WBVR	B	Kornilov et al. (1991)	4400	881	171	171
	V		5531	924	171	171
	R		7164	1312	171	171
	m35		3465	374	102	145
	m38		3825	327	122	185
DDO	*m41*	McClure (1976)	4164	80	124	191
	m42		4255	71	124	191
	m45		4520	73	124	191
	m48		4884	194	124	191
(RI)C	R	Cousins (1976)	6507	1479	65	81
	I		7904	1042	67	84
(RI)Eggen	R	Eggen (1965)	6350	1200	113	126
	I		7900	900	113	94
	J	Johnson & Morgan (1951),	12602	3268	87	154
IJHKLMN	H	Mendoza v. (1963),	16551	2607	89	144
	K	Bessell & Brett (1988)	22094	5569	44	79
Tycho[c]	B_T	Bessell & Murphy (2012)	4213	693	342	342
	V_T		5345	1043	342	342
Hipparcos[c]	H_p	Bessell & Murphy (2012)	5593	2471	346	346

NOTE. —Details of the photometric sample can be found in § 3.

[a] The effective width ($W_{\rm eff}$) is defined as: $W_{\rm eff} = (\int S_x(\lambda)d\lambda)/\max(S_x(\lambda))$. This is essentially the equivalent width divided by the maximum throughput within the filter bandpass.

[b] $N_{\rm ph}$ is the number of photometric points included in our analysis and $N_{\rm st}$ is the number of spectra with measurements in that filter. $N_{\rm ph} \geq N_{\rm sp}$ because many stars have more than one measurement in a given band.

[c] Tycho and *Hipparcos* are not in the GCPD, so we list their common names.

such as Alexander (Jones et al. 1981) and Oja (Häggkvist & Oja 1970), lack photometry for stars in our spectroscopic sample. To determine the minimum number of spectra required, we run our analysis (§ 4) on random subsets of the *UBV* filter sample. We find that if the subset contains $\lesssim 40$ spectra (independent of how many photometric points there are per spectrum) the resulting filter profile is frequently ($\gtrsim 30\%$ of the time) outside the range of profiles generated by our analysis of the full set (see § 5.2 for more details). We therefore require that to be included in our analysis a system/filter must have photometry for at least 40 stars in our spectroscopic sample and these $>= 40$ stars span at least 1 magnitude in $B - V$ color. We exclude Johnson R and I from our tests. Johnson I is not fully covered by either of our spectral libraries, and Cousins R and I (which we do test) are more commonly used compared to their Johnson counterparts. We list all photometric systems tested in this article in Table 1.

The GCPD differentiates between photometric systems even though they are in fact indistinguishable. The Straizys system (Kakaras et al. 1968) and Vilnius systems are identical; B and V from the Cape (GCPD name *UcBV*) system are in the Johnson system; GCPD systems *UBV* and *UBVE* are indistinguishable (Fig. 1); and (RI)C, Eggen, and *UBVRI* all contain Johnson U, B, and/or V measurements in addition to their own unique system measurements. For our purposes we analyze systems with identical or nearly identical parameters together.

Initially, we adopt the zero point and filter profile given in the GCPD (listed in Table 1). Many of these systems have been subsequently revised (e.g., Maíz Apellániz 2006; Bessell 2011; Bessell & Murphy 2012). However, our analysis only requires an approximate value for these as an initial guess. We compare our final filter profiles to updated literature values in § 5.

In addition to the photometry listed in Table 1 we analyze photometry from *Hipparcos* (van Leeuwen & Fantino 2005; van Leeuwen 2007), and Tycho-2 (Høg et al. 2000). We download

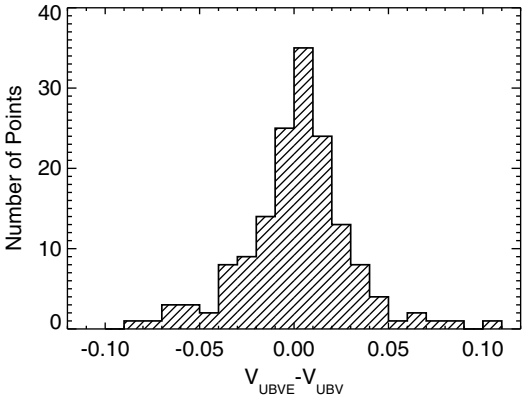

FIG. 1.—Comparison of V magnitudes from the GCPD *UBVE* and *UBV* systems. The median difference is 0.000, and the mean difference is 0.001 with a standard deviation of $\simeq 0.02$, which is consistent with measurement noise and/or stellar variability. Much of the photometry in the GCPD listed under different names are actually on the same system. See § 3 for details.

2MASS photometry (for the NIR data), although we do not attempt to derive new zero points or filter profiles for 2MASS, as the calibration of our NIR data is not sufficiently precise to improve upon the calibration from Cohen et al. (2003). Rather, 2MASS data is only included to improve the absolute flux calibration of the NIR spectra. For *Hipparcos* and Tycho-2 photometry we use the initial zero points and system sensitivities from Bessell & Murphy (2012) and for 2MASS we use those from Cohen et al. (1992, 2003).

As noted by Bessell & Murphy (2012) and Casagrande & VandenBerg (2014), there is some confusion in the literature regarding photonic (photon-counting) versus energy response functions. Since the bands are generally normalized the difference is a factor of $\int \lambda d\lambda$ (see eqs. [2] and [3] below), which can be very significant for broadband photometry. For references that provide ambiguous information we assume they report photonic filter profiles, as we found this gave better agreement with our final results. We convert all photonic response curves to energy response functions (more appropriately called system sensitivity, which we denote as S_x). The energy response is easier to use when calculating synthetic fluxes from flux-calibrated spectra (generally in energy units). For our derived filter profiles (§ 5, Appendix) we report energy response functions.

Photometry for each star is downloaded from the GCPD using the python script *GCPD3*.[6] Photometry from *Hipparcos*, Tycho-2, and 2MASS (with errors) are downloaded using the IDL routine *QUERYVIZIER*.[7]

4. ANALYSIS

Here, we compare the literature photometry with the flux-calibrated spectra and derive updated filter profiles, zero points, and photometric corrections.

4.1. Comparing Photometric Fluxes to Spectroscopic Fluxes

The synthetic flux ($f_{\mathrm{syn},x}$) is the flux in the sample spectrum, integrated over the filter profile, where the transmission of the filter is a wavelength-dependent quantity, and is calculated using the formula:

$$f_{\mathrm{syn},x} = \frac{\int f_\lambda(\lambda) S_x(\lambda) d\lambda}{\int S_x(\lambda) d\lambda}, \quad (2)$$

where f_λ is the flux-calibrated spectrum (e.g., erg cm^{-2} s^{-1} Å^{-1}) as a function of wavelength (λ).[8] $S_x(\lambda)$ is the system's *energy* sensitivity for the filter x (e.g., U, B, V), defined as:

[6] Please see https://github.com/awmann/GCPD3.

[7] Please see http://idlastro.gsfc.nasa.gov/ftp/pro/sockets/queryvizier.pro.

[8] The more appropriate term for f is radiative flux density or spectral irradiance, but for simplicity we use the more common astronomy term, flux or spectrum.

$$S(\lambda) = QE(\lambda)\lambda, \quad (3)$$

where $QE(\lambda)$ is the unit-less fractional transmission (i.e., photons detected/photons received). The combination of equations (2) and (3) put us in accord with equation (A11) from Bessell & Murphy (2012) and equation (3) from Bohlin et al. (2014). All synthetic fluxes are calculated using custom IDL routines, but we test to ensure consistency with the commonly used python tool *Pysynphot*.

Corresponding photometric fluxes from GCPD, *Hipparcos*, Tycho-2, and 2MASS photometry (denoted by $f_{\mathrm{phot},x}$) are computed using the formula:

$$f_{\mathrm{phot},x} = f_{0,x} 10^{-0.4(m_x)} \quad (4)$$

where m_x is the magnitude and $f_{0,x}$ is the zero point for band x. For this work, we use flux units (erg cm^{-1} s^{-2} Å^{-1}) rather than magnitudes when discussing zero points because they are more intuitive when discussing fractional differences (e.g., 30% is easier to imagine than 0.39 magnitudes) and because they are more practical for absolutely flux calibrating spectra. We report magnitudes where possible for reference.

In most cases, spectrophotometric libraries have precise *relative* flux calibrations (i.e., flux levels as a function of wavelength) but can still have significant absolute flux calibration errors (i.e., the whole spectrum is off by a constant). Bessell & Murphy (2012) solve this by renormalizing their spectra using precise *Hipparcos* (H_P) magnitudes. Instead, we renormalize using all available photometry, which is also more resistant against outlier photometry (e.g., taken during a flare) and enables us to include stars lacking H_P magnitudes. Specifically, after we compute synthetic and photometric fluxes we multiply each spectrum by a constant, C, which we define as:

$$C = \langle f_{\mathrm{phot},x} / f_{\mathrm{syn},x} \rangle, \quad (5)$$

where $\langle\,\rangle$ denotes the median, which we calculate over all bands (x) for a given star. This serves to absolutely flux calibrate each spectrum. The 1σ error on C is assumed to be the standard deviation of $f_{\mathrm{phot},x}/f_{\mathrm{syn},x}$ values after removing 5σ outliers. Note that although we are calibrating the spectrum using uncorrected (and possibly erroneous) photometry, our process for fixing the photometric parameters is iterative and converges quickly (see § 4.2 for more details). We show two example calibrated spectra in Figure 2 with the photometric fluxes for comparison.

In theory, it is possible to get a better C (and error estimate) using a robust weighted mean instead of a median. This is impractical because (1) measurement and zero point errors (and hence weights) for the GCPD photometry are not known, (2) while Tycho-2 and *Hipparcos* report measurement errors, zero point errors are not known, and (3) a median does a better job at ignoring outlier photometry when there are only $\simeq$5 measurements.

We show the distribution of corrections (C) applied to each of our libraries in Figure 3. The distribution similar to that derived for the NGSL library by Bessell & Murphy (2012), who renormalize their spectra using *Hipparcos* photometry alone. In general, the corrections are small for the NGSL library, but there are a number of outliers with $>20\%$ corrections. Most of these outliers are also seen in the distribution of renormalizations from Bessell & Murphy (2012), although many they identify appear to be cut by our variability criterion (See § 2). Corrections for the IRTF library often exceed 10%. Estimated errors on the normalization are also generally larger for the IRTF data ($\sim$1–3%) than for the NGSL library ($<1\%$). This is because there are typically only 5–6 photometric points for a given star in the NIR (2MASS JHK_S and Johnson *JHK*) while most of

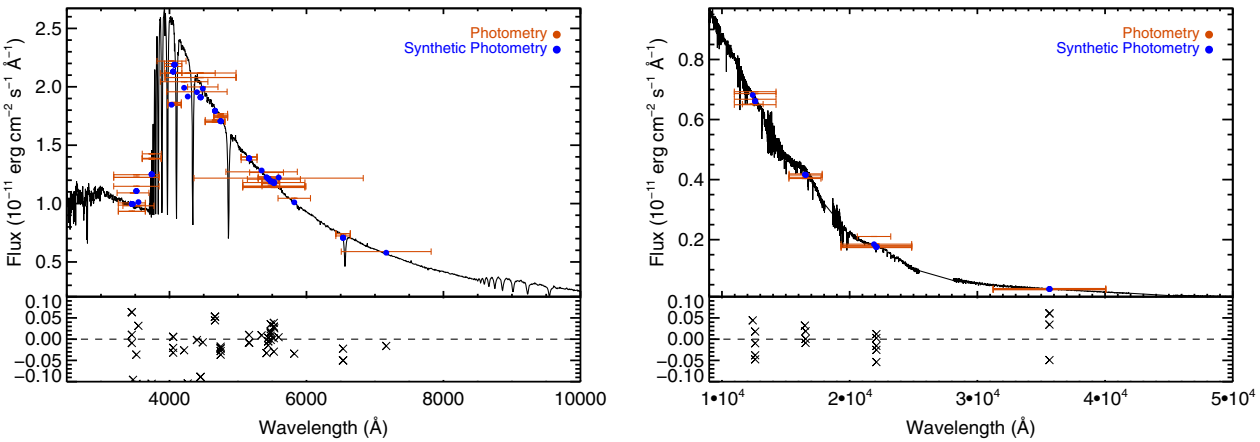

FIG. 2.—Demonstration of our flux calibration of the NGSL spectrum of the B9 dwarf HD 147550 (*left*) and the IRTF library spectrum of the M2 dwarf HD 95735 (*right*). Flux derived from photometry is shown in red with "error bars" showing the approximate FWHM of the filter profile. *Blue circles* indicate the corresponding flux estimated from the spectrum (synthetic flux). Fractional residuals (synthetic–photometric)/synthetic are shown on the bottom panel of each figure. See § 4.1 for more details. See the electronic edition of the *PASP* for a color version of this figure.

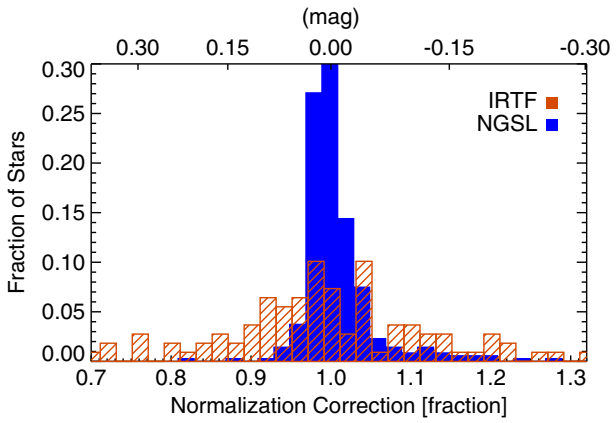

FIG. 3.—Distribution of normalizations applied to the NGSL and the IRTF library with the supplemental SpeX spectra. Five spectra have corrections >30% land outside the range of this plot, three of which are from our supplemental IRTF data. Changes in flux (as a fraction) are shown on the bottom X-axis with corrections in magnitudes on top for reference. See § 4.1 for more details on our procedure to absolutely flux calibrate the spectra. See the electronic edition of the *PASP* for a color version of this figure.

the NGSL stars have >30 photometric measurements, and because of lower precision flux calibration for the IRTF library.

Once the spectrum has been renormalized, we recalculate all synthetic fluxes following equation (2). We then examine the ratio of photometric to synthetic flux ($f_{\mathrm{phot},x}/f_{\mathrm{syn},x}$) as a function of $B-V$. $B-V$ magnitudes for each star are computed Tycho-2 B_T and V_T using the formula from Mamajek et al. (2002), where available. For stars lacking Tycho-2 magnitudes, we use $B-V$ colors from the GCPD. We use $B-V$ as a measure of color because it is the only color index that is available for all stars in our spectroscopic sample.

We find significant discrepancies between synthetic and photometric flux as a function of $B-V$ color (see Fig. 4 for two examples). The shape and amplitude of the trend with $B-V$ varies for each filter/system, but tends to be worse for filters with larger wavelength coverage (broader). Differences between photometric and spectroscopic fluxes of 10–20% are typical for broad filters and for the reddest and bluest stars. Both broad and narrow filters typically show systematic offsets (≃5–10%) from a (median) flux ratio of unity.

The trends we see in $f_{\mathrm{phot},x}/f_{\mathrm{syn},x}$ with $B-V$ can be explained by errors in the filter profile. For example, an optical filter profile that is redder than the true system throughput will include extra flux from an M star because the SED of the M star is increasing with wavelength over the filter passband, but miss flux from an A star because the SED is decreasing. We illustrate a simple version of this effect in Figure 5. More complicated trends like those seen in Figure 4*a* are the consequence of multiple, overlapping issues with the filter profile. Errors in width, shape, and central wavelength of the filter passband combined with nonsmooth spectra (e.g., a deep temperature sensitive feature somewhere in the passband) can give rise to such polynomial relations. We note that most filters show trends significantly closer to linear than what we see with Johnson U shown in Figure 4.

Although the trends are large they are also relatively tight; specifically, the scatter around a polynomial fit to the data is small. An examination of the outlier points indicates that many of the stars have additional discrepant photometry in the same filter, suggesting stellar variability or erroneous measurements can explain much of the scatter. Although we screened for known variables and tighter binaries, many will be missed. For statistical purposes we do not remove any of these outlier points.

The disagreement between photometric and spectroscopic fluxes decreases if we adopt more recent system parameters from the literature. For example, if we use filter profiles and zero points from Bessell & Murphy (2012) for the Johnson

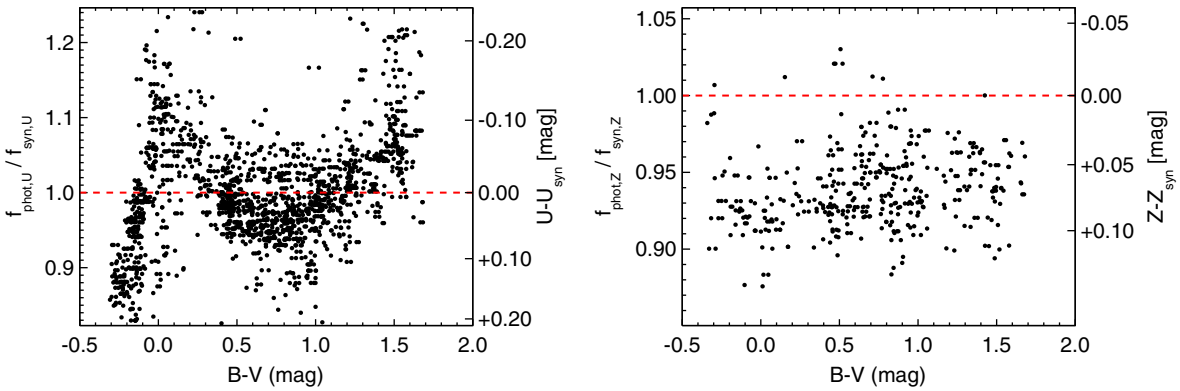

FIG. 4.—The ratio of flux from observed photometry (f_{phot}) to that calculated from the spectra (f_{syn}) as a function of $B-V$ color for Johnson U (*left*) and Vilnius Z (*right*). $B-V$ magnitudes are calculated from Tycho-2 B_T and V_T where available, and from the GCPD elsewhere. The magnitude differences is shown on the right Y-axis for reference. Note that the Y-axis scales of the two plots are not the same. The red dashed line indicates agreement between photometric and spectroscopic fluxes. We have added an artificial scatter of 0.025 magnitudes in $B-V$ to spread out overlapping points. See § 4.1 for more information. See the electronic edition of the *PASP* for a color version of this figure.

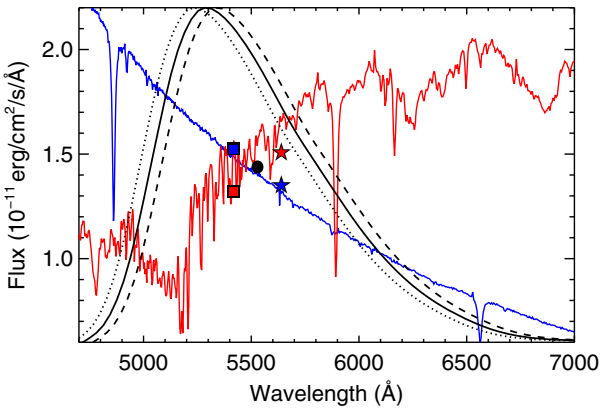

FIG. 5.—Example of how slightly inaccurate filter profiles create color-terms. We show the spectrum of the B6 star HD 174959 (*blue*) and the K7 star HD 201092 (*red*). These stars are selected because they have nearly identical V magnitudes. When we use the correct V filter profile (*solid black line*) the derived fluxes for both stars are nearly identical (*black dot*). If we shift the filter passband 1% redward (*dashed line*) the derived flux increases by $\simeq$6%, but decreases by $\simeq$6% for the B6 star (*red and blue stars*). The effect has a similar magnitude but opposite sign when we shift the filter blueward. More details can be found in § 4.1. See the electronic edition of the *PASP* for a color version of this figure.

U, B, and V filters the B and V synthetic and photometry-based fluxes agree at the level of $\simeq$2–6%, compared to 10–15% when using the GCPD parameters. Small trends with $B-V$ color are still present but only amount to 2–6% changes over 1.5 magnitudes in $B-V$. The improvement in U is much less significant (Fig. 6). This is most likely because Bessell & Murphy (2012) make use of the MILES library, which does not cover all of the U band. Instead they have to interpolate past the end of their spectra, which introduces error.

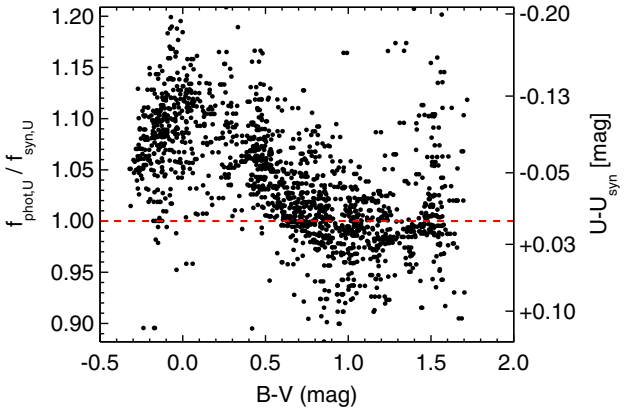

FIG. 6.—Similar to Figure 4 for the Johnson U band, but using the zero points and passbands are taken from Bessell & Murphy (2012). This is an improvement over the older system parameters but a significant trend is still seen. Note that the Y-axis scale is similar but not identical to that in Fig. 4. See the electronic edition of the *PASP* for a color version of this figure.

4.2. Deriving New System Parameters

We derive a new passbands and zero points for each band using a Monte Carlo (MC):

1. Adjust the filter profile's *shift*, *skew*, and *broad*, which we define according to the following equations:

$$\lambda_{\rm mod} = \lambda * {\rm shift} \tag{6}$$

$$\lambda_{\rm mod} = \lambda * ((\lambda - \lambda_{\rm peak}) + 1)^{\rm broad} \tag{7}$$

$$S_{\rm mod}(\lambda) = S(\lambda) * \lambda^{\rm skew}, \tag{8}$$

where $\lambda_{\rm mod}$ and $S_{\rm mod}$ are the wavelength and flux levels for the modified filter profile, and $\lambda_{\rm peak}$ is the wavelength of maximum flux transmission. Figure 7 shows how each of these parameters changes the overall profile.

2. Normalize filter profiles such that their maximum transmission is unity.

3. Recalculate synthetic fluxes ($f_{{\rm syn},x}$) for all stars from the calibrated spectra and the modified filter profile.

4. Flag and remove points with $f_{{\rm phot},x}/f_{{\rm syn},x}$ more than 5σ outside a 20-point running robust mean.

5. Calculate and apply a correction to zero point such that the median $f_{{\rm phot},x}/f_{{\rm syn},x}$ is 1.

6. Calculate the probability that $B-V$ is correlated with $f_{{\rm phot},x}/f_{{\rm syn},x}$ using a Spearman rank test (Spearman 1904).

7. Compute the rms scatter in $f_{{\rm phot},x}/f_{{\rm syn},x}$.

The above steps are repeated, each time adjusting the *shift*, *skew*, and/or *broad* parameters, which in turn alter the filter profile. *Shift* is varied from 0.9 to 1.1, *broad* from -2 to 2, and *skew*

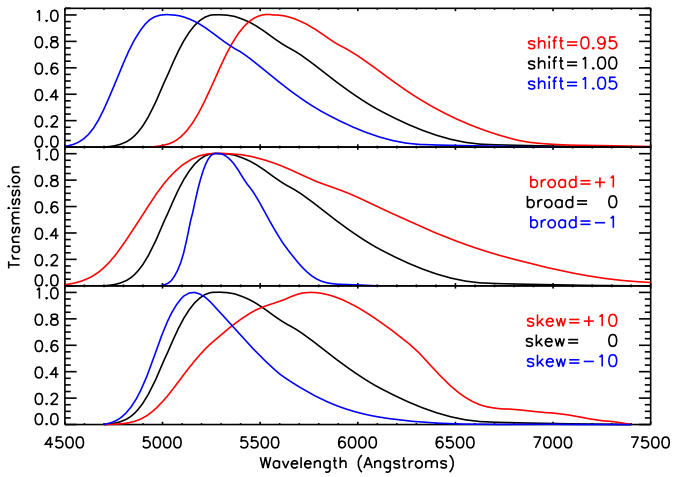

FIG. 7.—The effects of equations (5)–(7) on the filter profile. *Shift* moves the central wavelength, *broad* adjusts how narrow or broad the profile is, and *skew* changes relative transmission between the blue and red end of the profile. Relatively large values of each parameter are used for this figure to make the effect more clear. See the electronic edition of the *PASP* for a color version of this figure.

from -5 to 5, all in increments of 0.01. The range of values for *shift*, *skew* and *broad* are conservatively large (by design); none of our final filter profiles are near the limits for any parameter. After the MC is complete, we adopt the filter parameters that yield a $<50\%$ probability of a correlation with $B-V$ and the smallest scatter in $f_{\mathrm{phot},x}/f_{\mathrm{syn},x}$. We show illustrative examples of steps in the MC chain in Figure 8.

The Spearman rank test is best at identifying linear trends in the data. If there are significant nonlinear trends in the data, a Spearman rank test might find a low probability of correlation even for highly correlated data. We remedy this by splitting the data into two subsets along the median $B-V$ color and then recalculate the Spearman rank coefficient on each subset and for each MC step. We throw out profiles that show statistically significant correlation in either subset. Examination of remaining $f_{\mathrm{phot},x}/f_{\mathrm{syn},x}$ versus $B-V$ color plots suggests this method is sufficient to remove obvious poor profiles.

The absolute flux calibration factors we apply to each spectrum (see § 4.1, Fig. 3) are based on uncorrected photometry. Although C (eq. [5]) is calculated from the median of many points, the normalizations will still be slightly off due to errors in the filter parameters. To remedy this, we rederive the absolute flux calibration constant for each library spectrum using the updated filter parameters. The changes are generally small, with a median normalization change of 0.3%, but the largest changes are $>10\%$ (stars with few measurements or most measurements in the same filter), and show a trend with stellar color (the reddest and bluest stars change the most). After renormalizing the spectra with updated filter parameters we rerun the MC, deriving new filter profiles and zero points, this time with better-calibrated spectra. This process is repeated until changes in the derived zero points and filter profiles are negligible ($<0.1\%$). For most filters this happens after just 2–3 iterations, with the worst cases taking five iterations.

5. RESULTS

5.1. Updated Passbands and Zero Points

We list our final derived parameters for each system in Table 2. Zero points are given in erg $\mathrm{cm}^{-1}\,\mathrm{s}^{-2}\,\mathrm{\AA}^{-1}$, but can be converted to magnitudes using the formula:

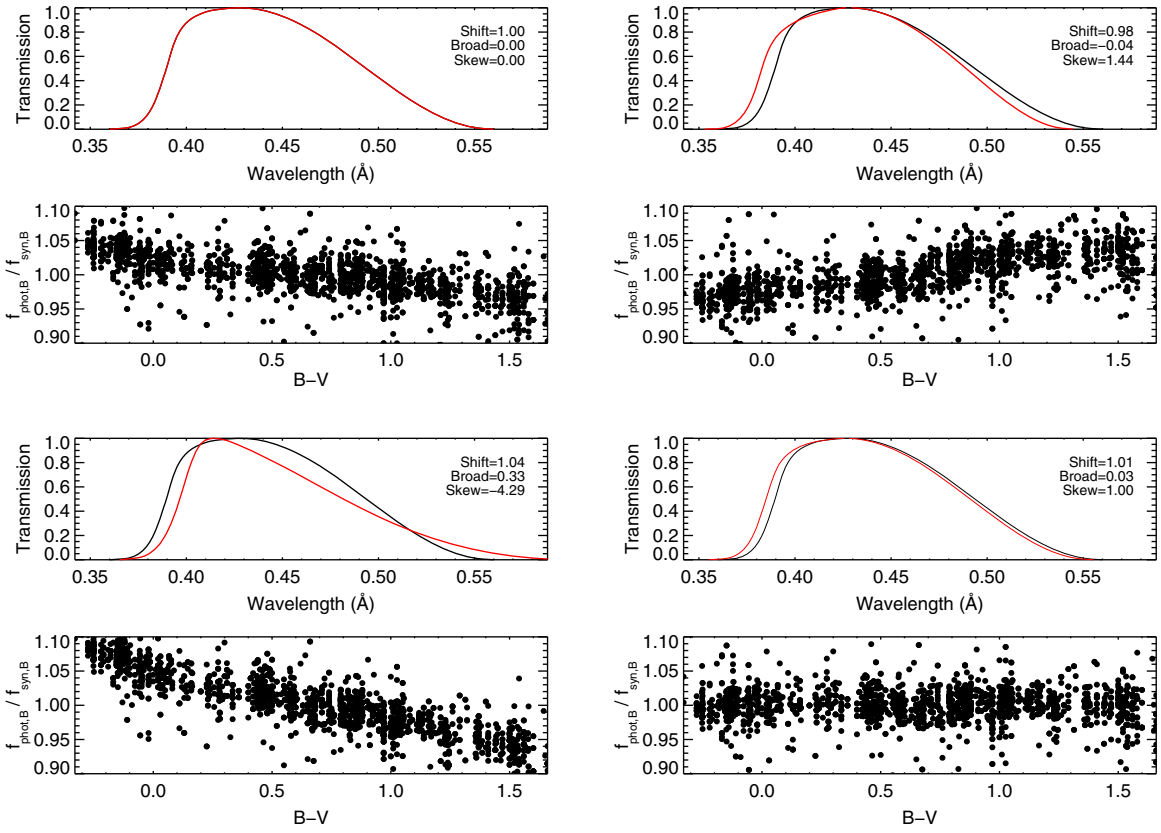

FIG. 8.—Four example steps in the MC chain for the Johnson B filter. The top of each panel shows the filter profile adopted by that step in red, with the initial input profile in black, along with the *skew*, *shift*, and *broad* parameters in the legend. The bottom of each panel is analogous to Figs. 4 and 6. Each panel represents a different step in the MC, with the top-left showing the initial value, and the bottom right showing the final result, and the other top-right and bottom-left displaying representative spots along the chain. Axis ranges are identical in all plots. Our MC procedure is described in § 4.2. See the electronic edition of the *PASP* for a color version of this figure.

TABLE 2
FINAL ZERO POINTS AND PASSBAND PARAMETERS

Name	Band	Zero point	±	Center	$W_{\rm eff}$
		10^{-9} erg cm^{-1} s^{-2} Å^{-1}		(Å)	
Cape	U_C	23.25	0.14	3925	999
	U	4.264	0.022	3620	1380
	B	6.459	0.032	4412	1816
Johnson	V	3.735	0.019	5529	1129
	J	0.310	0.003	12603	2095
	H	0.113	0.001	16552	1362
	K	0.0400	0.0005	22094	2142
	u	11.72	0.06	3485	950
Stromgren	b	5.974	0.030	4671	338
	v	8.691	0.044	4125	513
	y	3.778	0.019	5474	596
	U	5.612	0.029	3453	1404
	B1	6.676	0.034	4031	861
	B	2.838	0.014	4230	1523
Geneva	B2	10.76	0.05	4448	597
	V1	7.460	0.038	5379	788
	V	3.728	0.019	5495	1220
	G	9.462	0.048	5785	543
	U	18.75	0.10	3478	884
	P	14.30	0.08	3750	418
	X	11.28	0.06	4061	584
Vilnius	Y	6.792	0.035	4697	725
	Z	4.583	0.023	5204	244
	V	3.772	0.019	5464	584
	S	1.863	0.010	6520	271
	W	3.523	0.018	3554	963
WBVR	B	6.619	0.034	4382	1495
	V	3.730	0.019	5519	1394
	R	1.698	0.009	7166	1360
	m35	13.02	0.07	3521	1015
	m38	6.867	0.037	3864	709
DDO	m41	21.16	0.11	4182	211
	m42	19.97	0.10	4257	145
	m45	13.15	0.07	4512	141
	m48	4.966	0.025	4912	437
Cousins	R	2.215	0.012	6615	1877
	I	1.163	0.007	8047	1604
Eggen	R	2.293	0.016	6989	2831
	I	1.337	0.011	8492	1330
Tycho	Bt	6.798	0.034	4220	1455
	Vt	4.029	0.020	5350	1665
Hipparcos	Hp	3.926	0.020	5586	2569

NOTE. —Zero points are all derived from our MC analysis (see § 4). Errors are calculated from estimates of systematic errors in the flux calibration of our spectra and the standard error (see § 5.2). Full filter profiles are given in the Appendix.

$$ZP_{\rm mag} = -2.5\log(ZP_{\rm flux}) - 21.10. \quad (9)$$

Full normalized filter curves are given in the Appendix.

For Johnson *JHK* filters our derived passbands are indistinguishable from the original. Compared to other systems we examine, there is a paucity of measurements for *JHK* that overlap with our spectroscopic sample. Given this, and the larger errors associated with flux calibration of NIR data we decide to adopt the original filter profiles, but still adjust the zero points for these three filters.

In Figure 9, we show $f_{{\rm phot},x}/f_{{\rm syn},x}$ as a function of $B-V$ for two sample filters using our revised curves and zero points. Inspection of analogous plots for all filters and systems indicates that our profiles are removing systematic trends in the data.

In Figure 10, we show a comparison of the input (original) zero points to those derived from our MC analysis. Of the 42 filters tested, 32 change by $<5\%$, 6 change by 5–10%, and 4 change by $>10\%$. Input zero points are meant as an initial guess for the MC, and are not necessarily the best available. Thus we also compare to the more recent analysis of Bessell & Murphy (2012) for Johnson *UBV*, Cousins RI, *Hipparcos*, and Tycho-2 photometry. Our zero points are within 2% of those from Bessell & Murphy (2012), with the exception of the Johnson U filter, for which we disagree by 5%. We suspect the difference is due to their use of the MILES library, which does not cover the full U band.

In Figures 11, 12, and 13, we compare our derived filter profiles to those from Bessell (2011) and Bessell & Murphy (2012). The differences appear relatively small, but small differences can have a big impact for the bluest and reddest stars (see Figs. 4 and 6). Note that zero point and filter profile changes are also correlated. If we adopt the input filter profiles we derive zero points which are generally closer to the originals, but this reintroduces color-terms.

5.2. Understanding Errors

One important aspect of our analysis is to come up with an estimate for the error on the zero points. A simple method would be to calculate the standard error on the ratios of observed to synthetic fluxes ($f_{{\rm phot},x}/f_{{\rm syn},x}$). Because most bands have $\gg$100 points and the standard deviation of $f_{{\rm phot},x}/f_{{\rm syn},x}$ within a given filter tends to be small (1–3%), this method would suggest zero point errors $\lesssim 0.2\%$. This is unrealistically small because our analysis is dominated by systematic errors. In particular the largest source of error is errors in the spectrophotometric calibration of the NGSL or IRTF spectra.

Flux calibration better than 1% in the NIR is extraordinarily difficult because time-dependent changes in the sky (seeing, transmission, etc.) create wavelength-dependent flux losses that vary between target and standard observations. Cushing et al. (2005) and Rayner et al. (2009) mitigate for this by observing at the parallactic angle. By absolutely calibrating the library to 2MASS and comparing the residuals, Rayner et al. (2009) estimate that the IRTF library has spectral slopes accurate to 1–3%, although our own analysis suggests it is $\simeq 1\%$, and much of the variation actually arises because of larger errors in 2MASS photometry for the brightest stars (nonlinear part of the detector or saturation). Differences between 2MASS and the IRTF spectra

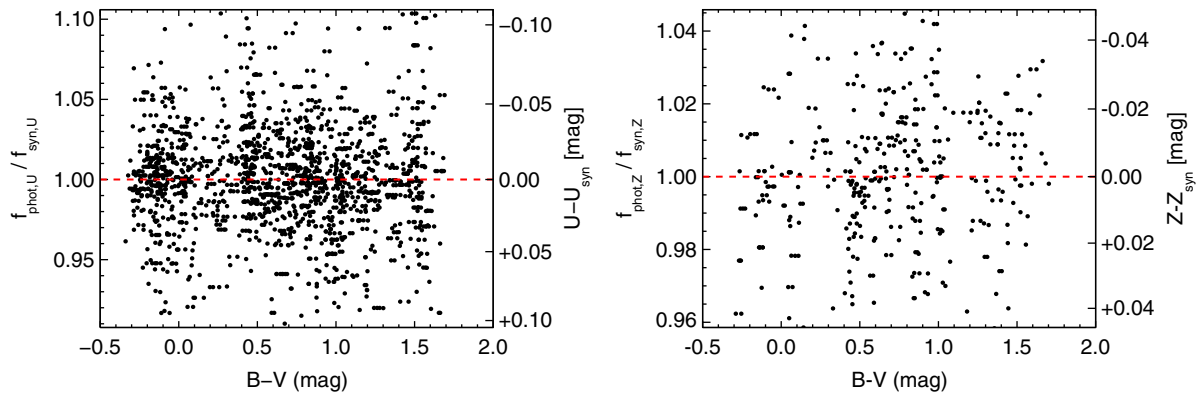

FIG. 9.—Similar to Fig. 4, but using our revised filter profiles and zero points. Note that the Y-axis scales of the two plots are not the same, nor are they the same as those in Fig. 4. For Z and U, respectively, there are three and eight outlier points outside the scale of the figures. These are most likely variable stars, erroneous measurements, or measurements assigned to the wrong star as the scatter in repeat measurements with the same filter on the same star is typically only 0.02–0.04 mags. The *red dashed line* indicates agreement between photometric and spectroscopic fluxes. Consult § 5.1 for more information. See the electronic edition of the *PASP* for a color version of this figure.

are consistent with random errors, but we cannot rule out (systematic) slope errors of 1%. To be conservative we add 1% errors in quadrature with the standard errors calculated for zero points on *JHK* photometry.

Space-based spectra should be able to achieve extremely accurate relative flux calibrations, since the major source of error for ground-based observations is removal of time-dependent noise from the sky (Young et al. 1991; Mann et al. 2011). However, the instrument and telescope can also introduce slope changes. In fact, an earlier version of the NGSL had significant errors in the spectral shape due to imperfect centering of the target on the slit. This was later calibrated out in postprocessing, but highlights the difficulties in precisely flux calibrating spectra.

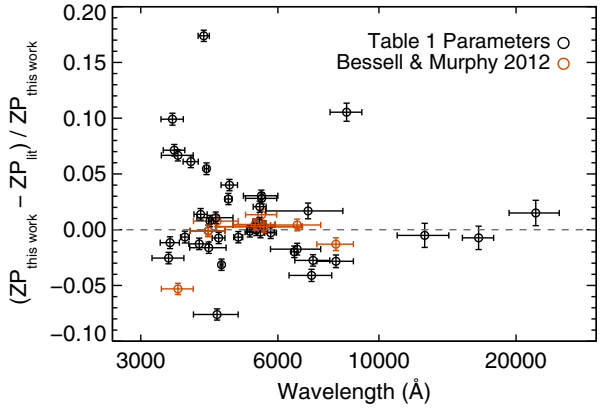

FIG. 10.—Fractional difference between zero points derived in this work and those from Table 1. *Horizontal error bars* indicate the $W_{\rm eff}$ for the given filter. *Vertical error bars* show the estimated error in our own zero points. While many filters change by $<5\%$, five change by more than 10%, including three off the scale of the figure. Zero points from Bessell & Murphy (2012) are shown (*red*) for reference. See § 5 for more details. See the electronic edition of the *PASP* for a color version of this figure.

To test the level of noise expected from shape errors we compare NGSL spectra with well flux-calibrated ground-based spectra from Mann et al. (2013b) for 10 overlapping stars (see Fig. 14 for an example). Slope differences are $<2\%$ in all cases, and on average are 0.9%. Mann et al. (2013b) report slope errors of 0.5–1% in their spectra based on repeat observations. This suggests most of the difference between the ground- and space-based spectra can be explained by errors in the ground-based data. With this small comparison sample we cannot rule out slope errors as large as 0.5%, so we conservatively add this to the standard errors on the zero points for all optical photometry. Final zero point errors are listed in Table 2 for all systems included in our analysis.

For any given filter our analysis produces a large number of acceptable filter profiles, i.e., profiles which have no statistically significant color terms and an rms in $f_{{\rm phot},x}/f_{{\rm syn},x}$ within a

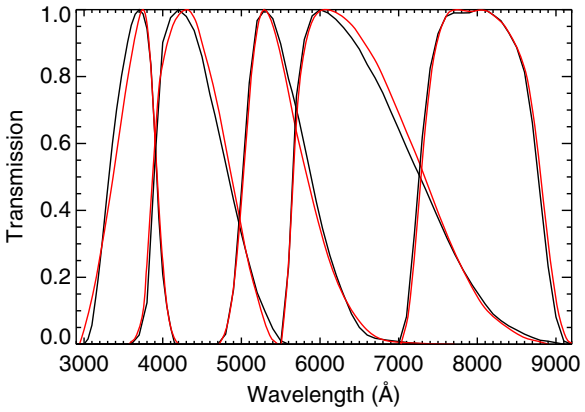

FIG. 11.—Filter response curves derived from our analysis (*red*) compared to those from Bessell & Murphy (2012) for Johnson *UBV* and Cousins *RI* filters. Note all filters are shown as energy response curves. See the electronic edition of the *PASP* for a color version of this figure.

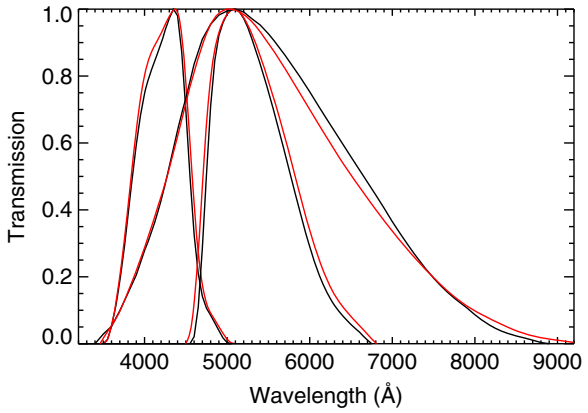

FIG. 12.—Same as Fig. 11 but for *Hipparcos* and Tycho-2 passbands. The broadest passband is the *Hipparcos* filter. See the electronic edition of the *PASP* for a color version of this figure.

factor of two of the smallest rms (we adopt the smallest rms as the true filter). In Figure 15, we show an example distribution of all acceptable filter profiles that comes out of our MC analysis. For all filters the distribution is similarly tight, which suggests that the adopted profiles are fairly reliable and that we are getting close to the real system parameters. This also suggests that errors on our derived filter profiles are relatively small.

6. SUMMARY AND DISCUSSION

In our effort to improve measurements of $F_{\rm bol}$ and, by extension $T_{\rm eff}$ and/or R_*, we tested the zero points and passbands for 42 different filters across a range of photometric systems. To this end we took advantage of the precise relative flux calibration of the NGSL and IRTF spectral libraries. By comparing flux calculated from the photometry to the corresponding flux in the spectrum we showed that errors in zero points and filter passbands can lead to flux errors of $>25\%$ for the bluest and reddest stars.

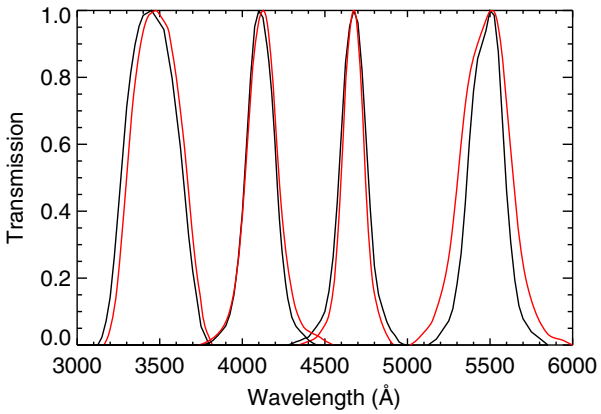

FIG. 13.—Same as Fig. 11 but for Strömgren (*ubvy*) passbands from Bessell (2011). See the electronic edition of the *PASP* for a color version of this figure.

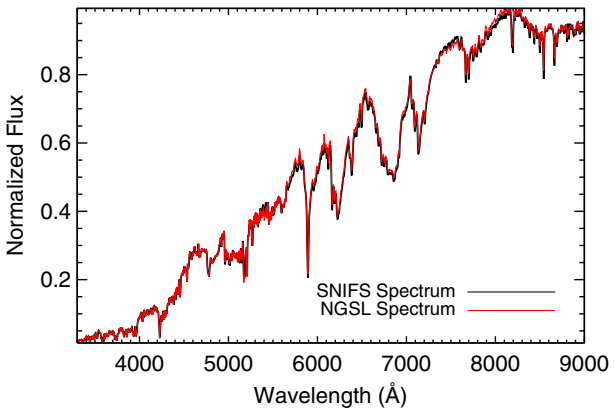

FIG. 14.—Ground-based optical spectrum (*black*) taken from Mann et al. (2013b) compared to a STIS spectrum (*red*) from NGSL of the star HD 1326 (GJ 15A). Both spectra have been normalized to their peak value. The differences in slope are $\simeq$1%, which is consistent with expected errors from SNIFS. See § 5.2 for more information. See the electronic edition of the *PASP* for a color version of this figure.

To derive new passbands and zero points, we ran an MC analysis on each of the 42 filters in our sample. The MC found the filter parameters that produce the best agreement between spectroscopic and photometric fluxes free of correlations with the color of the star. For most bands the changes were relatively small (e.g., $<5\%$ in zero points), but some changed by $>10\%$. Changes in filter profiles were also generally small, but still had a very significant effect on stars with extreme colors, and hence are important to avoiding systematic errors.

We estimated errors in our zero points by considering possible shape (relative flux calibration) errors in the NGSL and

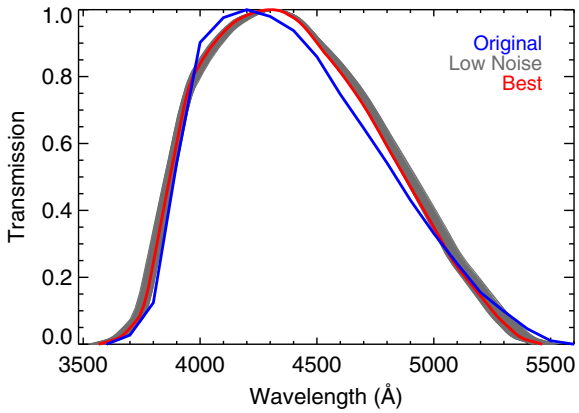

FIG. 15.—Filter profile for the Johnson B filter with original denoted in *blue*, and the best (adopted) profile shown in *red*. All filter profiles that show no correlation between $f_{{\rm phot},x}/f_{{\rm syn},x}$ and $B-V$ and have an rms in $f_{{\rm phot},x}/f_{{\rm syn},x}$ less than double the minimum rms (ones we consider acceptable solutions) that came out of our MC analysis are shown in *gray*. The original filter has been converted to energy response (as opposed to photon counting) for consistency with our analysis. See § 5.2 for more information. See the electronic edition of the *PASP* for a color version of this figure.

IRTF spectra. Based on a comparison to spectra from other sources, we estimated that the relative flux calibration of the NGSL library is good to $\lesssim 0.5\%$, although this may be a conservative estimate. For the IRTF spectra, the flux calibration is worse because of the complications involved in flux calibration NIR spectra from the ground. We expect that zero points for NIR filters are still good to $\simeq 1\%$ for most bands.

We also have estimated errors on the filter profiles by considering the range of reasonable filter profiles that come out of our MC analysis (Fig. 15). We report these errors alongside our derived filter profiles in the Appendix. However, readers are cautioned that these errors are highly correlated. For example, if we adopt transmission values lower than the best-fit value for the red end of the filter, then it is likely we will have to reduce the throughput in the blue in order to avoid introducing a color term.

Our analysis has assumed that the true filter profile is a simple correction to the original profile. More complicated changes are more difficult to take into account because it makes parameter space too wide for the number of data points. For example, red leaks, which are common for blue filters, can easily give rise to color terms like those seen in this article. However, most CCDs optimized for blue filters have low quantum efficiency in the red, and hence are only mildly affected by red leaks. Given that we are able to derive filter profiles free of color terms even for photometry taken from different sources, using different detectors and optical systems suggests that few, if any of these filters are subject to very significant red leaks. Future analysis with additional spectra will enable us to search using more complicated filter profiles and confirm this suggestion empirically.

The presented revisions (see Table 2) are derived based on data in our spectroscopic sample that span the range $-0.4 \lesssim B - V \lesssim 1.7$. Consequently, we caution the reader that there may be color-terms in the filter profiles that only become apparent at more extreme red and blue colors.

We note that our derived system sensitivities are not necessarily the true profile. It is certainly possible that a system sensitivity could produce no color terms and still not match the original standards, although this raises the issue of whether it is possible to define a true system in an absolute sense. Original system definitions are rarely determined with the precision we can achieve today. It is unlikely that CCDs and filters installed are perfect clones of the original system, and even if they were, filters/instruments are often changed and observations are corrected using imperfect transformations to put data back onto the standard systems. This data amalgamation makes it difficult to define a single system sensitivity that describes all the photometry. However, narrow range of system profiles that comes out of our MC analysis is promising, and suggestive that even if our parameters do not match the original system they are useful and accurate for calculating synthetic photometry and fluxes.

Future efforts to calibrate NIR photometry will require spectra with better spectrophotometric calibration. The X-Shooter library (Chen et al. 2011) offers a special advantage because it is build from optical and NIR spectra taken simultaneously. In this case, optical photometry can be used to absolutely flux calibrate the spectrum, and then the NIR region can be used to independently test the NIR photometry. Unfortunately, the currently available version of the X-shooter library contains only optical data. Another advance will come with the expansion of the NGSL library (*HST* approved program ID 13776). This is expected to widen the color of the sample and provide an opportunity to revise/test the spectrophotometric calibration.

One of the primary motivations of this study was to significantly improve on the precision and accuracy of derived bolometric fluxes for stars observed with long-baseline optical interferometry. The shifts in filter profiles are especially important for this, because color terms will lead to systematic differences in the absolute photometry. This will correspondingly shift the absolute flux calibration, and hence, the derived $F_{\rm bol}$ and $T_{\rm eff}$ for any given star.

We highlight this point by recalculating $F_{\rm bol}$ for the K and M dwarfs from Boyajian et al. (2012) and Mann et al. (2013b), first using the original system parameters and then using the updated parameters from this work. We follow the same procedure to flux calibrate the spectra, i.e., use the median correction from all available photometry. As in Mann et al. (2013b), we extrapolate beyond the edges of the spectrum using a Rayleigh–Jeans law or Wien's approximation for the red and blue end, respectively. The $F_{\rm bol}$ is then calculated from the numerical integral of the entire spectrum. In Figure 16, we show the comparison of $F_{\rm bol}$ using old and new photometric system parameters. There is a clear systematic offset caused by the differences in absolute flux calibrations. This amounts to a median offset of 3%, which is statistically significant for most stars, and is highly significant if we consider the full sample. Further, the offset is larger for the

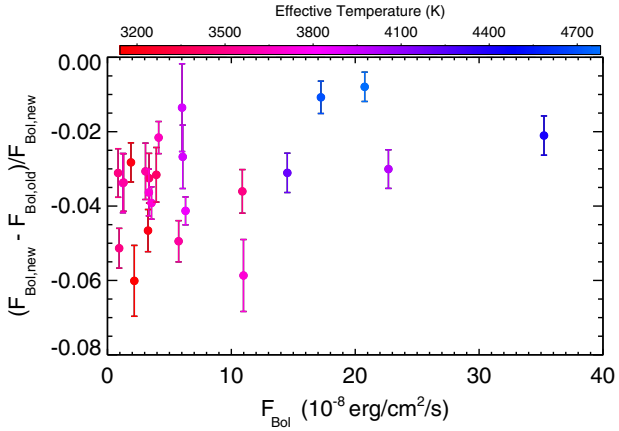

FIG. 16.—Values of $F_{\rm bol}$ calculated using updated parameters from this work (new) compared to those calculated using the original input parameters (old). Errors are calculated from the scatter in the normalization and measurement errors in the spectrum. See the electronic edition of the *PASP* for a color version of this figure.

coolest (reddest) stars (3–7%), emphasizing the importance of accurate photometric system parameters to reducing systematic errors.

The authors thank the anonymous referee for their extremely quick and useful review of our work. We also thank Megan Ansdell, Eric Gaidos, and Chao-Ling Hung for their useful comments on this manuscript. We give additional to thanks Simon Murphy, Tabetha Boyajian, and Gerard van Belle for their useful discussions at Cool Stars 18. This work was supported by the Harlan J. Smith Fellowship from the University of Texas at Austin to AWM.

This research has made use of the SIMBAD database, operated at CDS, Strasbourg, France. This work is based on observations made with the NASA/ESA Hubble Space Telescope, obtained at the Space Telescope Science Institute, which is operated by the Association of Universities for Research in Astronomy, Inc., under NASA contract NAS 5-26555. These observations are associated with GO program 11652.

APPENDIX

Please see Tables 3–13 for our final filter profiles.

TABLE 3

ENERGY RESPONSE FUNCTIONS, $S_x(\lambda)$, FOR JOHNSON

U		B		V	
λ Å	Trans	λ Å	Trans	λ Å	Trans
2942.0	0.000	3566.0	0.000	4718.2	0.000
2959.1	0.012	3591.6	0.005	4758.6	0.017
2976.2	0.024	3617.3	0.010	4799.1	0.041
2993.3	0.037	3642.9	0.016	4839.5	0.078
3010.4	0.051	3668.6	0.027	4880.0	0.134
3027.5	0.066	3694.2	0.044	4920.4	0.211
3044.6	0.082	3719.9	0.064	4960.8	0.311
3061.7	0.098	3745.5	0.092	5001.3	0.429
3078.8	0.115	3771.2	0.148	5041.7	0.553
3095.9	0.133	3796.8	0.232	5082.2	0.675
3113.0	0.152	3822.5	0.325	5122.6	0.788
3130.1	0.172	3848.1	0.419	5163.0	0.879
3147.2	0.192	3873.8	0.510	5203.5	0.943
3164.3	0.212	3899.4	0.599	5243.9	0.983
3181.5	0.234	3925.0	0.688	5284.4	1.000
3198.6	0.256	3950.7	0.763	5324.8	0.993
3215.7	0.279	3976.3	0.810	5365.3	0.975
3232.8	0.302	4002.0	0.839	5405.7	0.949
3249.9	0.325	4027.6	0.869	5446.1	0.915
3267.0	0.349	4053.3	0.895	5486.6	0.877
3284.1	0.373	4078.9	0.916	5527.0	0.835
3301.2	0.398	4104.6	0.936	5567.5	0.790
3318.3	0.423	4130.2	0.954	5607.9	0.742
3335.4	0.449	4155.9	0.967	5648.4	0.694
3352.5	0.475	4181.5	0.977	5688.8	0.648
3369.6	0.501	4207.2	0.985	5729.2	0.605
3386.7	0.528	4232.8	0.992	5769.7	0.565
3403.8	0.556	4258.5	0.996	5810.1	0.525
3420.9	0.583	4284.1	0.999	5850.6	0.486
3438.0	0.611	4309.8	1.000	5891.0	0.446
3455.1	0.639	4335.4	0.998	5931.4	0.407
3472.2	0.667	4361.1	0.991	5971.9	0.370
3489.3	0.695	4386.7	0.981	6012.3	0.334
3506.4	0.722	4412.3	0.970	6052.8	0.301
3523.5	0.749	4438.0	0.954	6093.2	0.270
3540.6	0.775	4463.6	0.933	6133.7	0.240
3557.8	0.800	4489.3	0.910	6174.1	0.214
3574.9	0.824	4514.9	0.887	6214.5	0.189
3592.0	0.847	4540.6	0.865	6255.0	0.167
3609.1	0.870	4566.2	0.843	6295.4	0.146
3626.2	0.892	4591.9	0.821	6335.9	0.128
3643.3	0.913	4617.5	0.797	6376.3	0.111
3660.4	0.933	4643.2	0.772	6416.7	0.096
3677.5	0.952	4668.8	0.746	6457.2	0.082
3694.6	0.970	4694.5	0.719	6497.6	0.069
3711.7	0.985	4720.1	0.691	6538.1	0.058
3728.8	0.996	4745.8	0.660	6578.5	0.047
3745.9	1.000	4771.4	0.628	6619.0	0.038
3763.0	0.997	4797.1	0.595	6659.4	0.030
3780.1	0.985	4822.7	0.564	6699.8	0.024
3797.2	0.962	4848.3	0.533	6740.3	0.019
3814.3	0.929	4874.0	0.502	6780.7	0.015
3831.4	0.885	4899.6	0.471	6821.2	0.012
3848.5	0.830	4925.3	0.440	6861.6	0.010
3865.6	0.767	4950.9	0.410	6902.1	0.008
3882.7	0.697	4976.6	0.378	6942.5	0.007
3899.8	0.625	5002.2	0.347	6982.9	0.006
3917.0	0.552	5027.9	0.316	7023.4	0.006
3934.1	0.481	5053.5	0.284	7063.8	0.005
3951.2	0.413	5079.2	0.253	7104.3	0.004
3968.3	0.349	5104.8	0.226	7144.7	0.004
3985.4	0.290	5130.5	0.204	7185.1	0.003
4002.5	0.238	5156.1	0.182	7225.6	0.003
4019.6	0.191	5181.8	0.160	7266.0	0.003
4036.7	0.151	5207.4	0.138	7306.5	0.002
4053.8	0.117	5233.1	0.116	7346.9	0.002
4070.9	0.089	5258.7	0.094	7387.4	0.002
4088.0	0.066	5284.4	0.074	7427.8	0.001
4105.1	0.047	5310.0	0.057	7468.2	0.001
4122.2	0.033	5335.6	0.041	7508.7	0.001
4139.3	0.022	5361.3	0.026	7549.1	0.001
4156.4	0.013	5386.9	0.016	7589.6	0.000
4173.5	0.008	5412.6	0.010	7630.0	0.000
4190.6	0.003	5438.2	0.005	7670.4	0.000

TABLE 3 (*Continued*)

TABLE 4

ENERGY RESPONSE FUNCTIONS, $S_x(\lambda)$, FOR CAPE

U	
λ (Å)	Trans
3190.4	0.000
3215.4	0.003
3240.3	0.006
3265.3	0.009
3290.3	0.012
3315.3	0.014
3340.3	0.017
3365.3	0.021
3390.2	0.030
3415.2	0.043
3440.2	0.065
3465.2	0.098
3490.2	0.139
3515.2	0.188
3540.1	0.246
3565.1	0.309
3590.1	0.379
3615.1	0.452
3640.1	0.527
3665.1	0.604
3690.0	0.679
3715.0	0.751
3740.0	0.820
3765.0	0.880
3790.0	0.931
3814.9	0.969
3839.9	0.991
3864.9	1.000
3889.9	0.986
3914.9	0.950
3939.9	0.897
3964.8	0.820
3989.8	0.726
4014.8	0.626
4039.8	0.522
4064.8	0.422
4089.8	0.339

TABLE 4 (*Continued*)

U	
λ (Å)	Trans
4114.7	0.275
4139.7	0.222
4164.7	0.186
4189.7	0.163
4214.7	0.143
4239.7	0.129
4264.6	0.118
4289.6	0.109
4314.6	0.102
4339.6	0.096
4364.6	0.091
4389.6	0.088
4414.5	0.086
4439.5	0.085
4464.5	0.086
4489.5	0.088
4514.5	0.092
4539.5	0.097
4564.4	0.101
4589.4	0.106
4614.4	0.110
4639.4	0.113
4664.4	0.114
4689.3	0.113
4714.3	0.110
4739.3	0.105
4764.3	0.098
4789.3	0.090
4814.3	0.080
4839.2	0.070
4864.2	0.059
4889.2	0.048
4914.2	0.039
4939.2	0.030
4964.2	0.022
4989.1	0.014
5014.1	0.007

TABLE 5

ENERGY RESPONSE FUNCTIONS, $S_x(\lambda)$, FOR DDO

*m*35		*m*38		*m*41		*m*42		*m*45		*m*48	
λ (Å)	Trans	λ (Å)	Trans	λ (Å)	Trans	λ (Å)	Trans	λ (Å)	Trans	λ (Å)	Trans
3166.1	0.000	3605.5	0.000	4094.0	0.000	4199.0	0.000	4454.2	0.000	4695.1	0.000
3176.1	0.004	3613.0	0.011	4096.4	0.002	4200.7	0.003	4455.9	0.004	4700.8	0.008
3186.1	0.008	3620.6	0.024	4098.8	0.004	4202.3	0.005	4457.6	0.008	4706.4	0.013
3196.1	0.017	3628.1	0.041	4101.2	0.006	4204.0	0.010	4459.2	0.013	4712.1	0.016
3206.1	0.030	3635.6	0.063	4103.6	0.010	4205.7	0.016	4460.9	0.019	4717.7	0.019
3216.1	0.047	3643.2	0.090	4106.0	0.015	4207.3	0.023	4462.6	0.026	4723.4	0.023
3226.1	0.071	3650.7	0.121	4108.4	0.022	4209.0	0.030	4464.2	0.035	4729.0	0.028
3236.1	0.102	3658.2	0.158	4110.8	0.030	4210.6	0.037	4465.9	0.048	4734.7	0.035
3246.1	0.137	3665.8	0.200	4113.3	0.039	4212.3	0.050	4467.6	0.066	4740.3	0.044
3256.1	0.181	3673.3	0.246	4115.7	0.051	4214.0	0.074	4469.2	0.094	4746.0	0.056
3266.1	0.228	3680.8	0.295	4118.1	0.067	4215.6	0.105	4470.9	0.131	4751.6	0.068
3276.1	0.279	3688.4	0.346	4120.5	0.089	4217.3	0.145	4472.6	0.182	4757.3	0.084
3286.1	0.332	3695.9	0.399	4122.9	0.117	4219.0	0.194	4474.2	0.248	4762.9	0.104
3296.1	0.386	3703.4	0.451	4125.3	0.153	4220.6	0.252	4475.9	0.322	4768.6	0.130
3306.1	0.443	3711.0	0.504	4127.7	0.196	4222.3	0.324	4477.6	0.402	4774.2	0.161

TABLE 5 (*Continued*)

*m*35		*m*38		*m*41		*m*42		*m*45		*m*48	
λ (Å)	Trans	λ (Å)	Trans	λ (Å)	Trans	λ (Å)	Trans	λ (Å)	Trans	λ (Å)	Trans
3316.1	0.501	3718.5	0.554	4130.1	0.246	4223.9	0.408	4479.2	0.487	4779.9	0.202
3326.1	0.555	3726.0	0.603	4132.5	0.309	4225.6	0.497	4480.9	0.576	4785.5	0.254
3336.1	0.606	3733.5	0.650	4134.9	0.387	4227.3	0.589	4482.5	0.670	4791.1	0.317
3346.1	0.653	3741.1	0.695	4137.3	0.477	4228.9	0.681	4484.2	0.762	4796.8	0.394
3356.1	0.699	3748.6	0.737	4139.7	0.563	4230.6	0.766	4485.9	0.831	4802.4	0.482
3366.1	0.742	3756.1	0.776	4142.1	0.645	4232.3	0.842	4487.5	0.880	4808.1	0.575
3376.1	0.782	3763.7	0.813	4144.6	0.723	4233.9	0.906	4489.2	0.916	4813.7	0.669
3386.1	0.817	3771.2	0.845	4147.0	0.798	4235.6	0.941	4490.9	0.935	4819.4	0.757
3396.1	0.848	3778.7	0.873	4149.4	0.864	4237.2	0.958	4492.5	0.945	4825.0	0.835
3406.2	0.877	3786.3	0.898	4151.8	0.911	4238.9	0.968	4494.2	0.951	4830.7	0.894
3416.2	0.905	3793.8	0.921	4154.2	0.943	4240.6	0.969	4495.9	0.954	4836.3	0.938
3426.2	0.930	3801.3	0.941	4156.6	0.963	4242.2	0.966	4497.5	0.957	4842.0	0.968
3436.2	0.948	3808.9	0.958	4159.0	0.972	4243.9	0.962	4499.2	0.962	4847.6	0.984
3446.2	0.960	3816.4	0.971	4161.4	0.978	4245.5	0.958	4500.9	0.969	4853.3	0.994
3456.2	0.970	3823.9	0.982	4163.8	0.983	4247.2	0.954	4502.5	0.976	4858.9	0.999
3466.2	0.980	3831.5	0.990	4166.2	0.987	4248.9	0.952	4504.2	0.984	4864.6	1.000
3476.2	0.988	3839.0	0.995	4168.6	0.990	4250.5	0.953	4505.9	0.991	4870.2	1.000
3486.2	0.994	3846.5	0.999	4171.0	0.993	4252.2	0.956	4507.5	0.996	4875.9	0.999
3496.2	0.998	3854.0	1.000	4173.4	0.995	4253.9	0.963	4509.2	0.999	4881.5	0.998
3506.2	1.000	3861.6	0.999	4175.9	0.997	4255.5	0.971	4510.9	1.000	4887.1	0.997
3516.2	1.000	3869.1	0.996	4178.3	0.998	4257.2	0.979	4512.5	0.996	4892.8	0.996
3526.2	0.999	3876.6	0.992	4180.7	0.999	4258.8	0.984	4514.2	0.989	4898.4	0.995
3536.2	0.995	3884.2	0.986	4183.1	1.000	4260.5	0.990	4515.8	0.981	4904.1	0.994
3546.2	0.988	3891.7	0.977	4185.5	1.000	4262.2	0.994	4517.5	0.973	4909.7	0.993
3556.2	0.979	3899.2	0.966	4187.9	0.999	4263.8	0.999	4519.2	0.964	4915.4	0.992
3566.2	0.969	3906.8	0.950	4190.3	0.998	4265.5	1.000	4520.8	0.956	4921.0	0.991
3576.2	0.956	3914.3	0.932	4192.7	0.996	4267.1	0.998	4522.5	0.950	4926.7	0.991
3586.2	0.941	3921.8	0.909	4195.1	0.995	4268.8	0.994	4524.2	0.944	4932.3	0.990
3596.2	0.923	3929.4	0.882	4197.5	0.993	4270.5	0.983	4525.8	0.942	4938.0	0.988
3606.2	0.903	3936.9	0.852	4199.9	0.990	4272.1	0.968	4527.5	0.942	4943.6	0.987
3616.2	0.881	3944.4	0.820	4202.3	0.986	4273.8	0.946	4529.2	0.940	4949.3	0.986
3626.2	0.857	3952.0	0.788	4204.7	0.981	4275.5	0.915	4530.8	0.937	4954.9	0.983
3636.2	0.830	3959.5	0.758	4207.2	0.974	4277.1	0.878	4532.5	0.931	4960.6	0.977
3646.2	0.800	3967.0	0.725	4209.6	0.962	4278.8	0.836	4534.2	0.916	4966.2	0.969
3656.3	0.768	3974.5	0.686	4212.0	0.932	4280.4	0.788	4535.8	0.891	4971.9	0.955
3666.3	0.733	3982.1	0.643	4214.4	0.886	4282.1	0.734	4537.5	0.852	4977.5	0.934
3676.3	0.697	3989.6	0.601	4216.8	0.824	4283.8	0.669	4539.2	0.786	4983.1	0.903
3686.3	0.660	3997.1	0.559	4219.2	0.752	4285.4	0.595	4540.8	0.698	4988.8	0.866
3696.3	0.620	4004.7	0.517	4221.6	0.671	4287.1	0.522	4542.5	0.606	4994.4	0.822
3706.3	0.576	4012.2	0.475	4224.0	0.582	4288.8	0.454	4544.2	0.508	5000.1	0.762
3716.3	0.530	4019.7	0.433	4226.4	0.492	4290.4	0.389	4545.8	0.412	5005.7	0.687
3726.3	0.482	4027.3	0.392	4228.8	0.405	4292.1	0.325	4547.5	0.328	5011.4	0.609
3736.3	0.432	4034.8	0.352	4231.2	0.325	4293.7	0.265	4549.1	0.259	5017.0	0.532
3746.3	0.383	4042.3	0.312	4233.6	0.257	4295.4	0.210	4550.8	0.199	5022.7	0.457
3756.3	0.336	4049.9	0.271	4236.0	0.203	4297.1	0.168	4552.5	0.151	5028.3	0.385
3766.3	0.290	4057.4	0.234	4238.5	0.161	4298.7	0.135	4554.1	0.114	5034.0	0.323
3776.3	0.246	4064.9	0.201	4240.9	0.130	4300.4	0.108	4555.8	0.085	5039.6	0.270
3786.3	0.207	4072.5	0.172	4243.3	0.107	4302.0	0.087	4557.5	0.066	5045.3	0.226
3796.3	0.170	4080.0	0.145	4245.7	0.088	4303.7	0.070	4559.1	0.052	5050.9	0.189
3806.3	0.137	4087.5	0.121	4248.1	0.071	4305.4	0.057	4560.8	0.041	5056.6	0.160
3816.3	0.106	4095.0	0.099	4250.5	0.056	4307.0	0.046	4562.5	0.033	5062.2	0.135
3826.3	0.080	4102.6	0.080	4252.9	0.042	4308.7	0.036	4564.1	0.027	5067.9	0.114
3836.3	0.058	4110.1	0.063	4255.3	0.031	4310.4	0.028	4565.8	0.022	5073.5	0.094
3846.3	0.039	4117.6	0.048	4257.7	0.022	4312.0	0.021	4567.5	0.018	5079.1	0.078
3856.3	0.025	4125.2	0.036	4260.1	0.017	4313.7	0.015	4569.1	0.014	5084.8	0.065
3866.3	0.015	4132.7	0.026	4262.5	0.012	4315.3	0.011	4570.8	0.010	5090.4	0.052
3876.3	0.009	4140.2	0.017	4264.9	0.009	4317.0	0.008	4572.5	0.007	5096.1	0.040
3886.3	0.004	4147.8	0.011	4267.3	0.006	4318.7	0.005	4574.1	0.004	5101.7	0.026
3896.4	0.002	4155.3	0.005	4269.8	0.003	4320.3	0.002	4575.8	0.002	5107.4	0.013

TABLE 6

ENERGY RESPONSE FUNCTIONS, $S_x(\lambda)$, FOR EGGEN

R		*I*	
λ (Å)	Trans	λ (Å)	Trans
5010.7	0.000	7309.7	0.000
5071.3	0.001	7349.2	0.004
5131.9	0.004	7388.6	0.009
5192.5	0.012	7428.0	0.019
5253.1	0.026	7467.4	0.034
5313.7	0.055	7506.8	0.055
5374.3	0.116	7546.3	0.083
5434.9	0.221	7585.7	0.118
5495.5	0.379	7625.1	0.164
5556.1	0.529	7664.5	0.236
5616.7	0.618	7704.0	0.353
5677.3	0.677	7743.4	0.529
5737.9	0.721	7782.8	0.699
5798.5	0.752	7822.2	0.805
5859.1	0.777	7861.7	0.863
5919.7	0.799	7901.1	0.909
5980.3	0.818	7940.5	0.943
6040.9	0.836	7979.9	0.967
6101.5	0.852	8019.4	0.985
6162.1	0.865	8058.8	0.995
6222.7	0.876	8098.2	0.999
6283.2	0.888	8137.6	1.000
6343.8	0.899	8177.1	0.997
6404.4	0.910	8216.5	0.990
6465.0	0.919	8255.9	0.977
6525.6	0.928	8295.3	0.958
6586.2	0.938	8334.8	0.936
6646.8	0.948	8374.2	0.913
6707.4	0.956	8413.6	0.887
6768.0	0.964	8453.0	0.861
6828.6	0.972	8492.4	0.835
6889.2	0.978	8531.9	0.810
6949.8	0.984	8571.3	0.785
7010.4	0.990	8610.7	0.761
7071.0	0.995	8650.1	0.737
7131.6	0.997	8689.6	0.712
7192.2	0.998	8729.0	0.689
7252.8	0.999	8768.4	0.666
7313.4	0.999	8807.8	0.646
7374.0	1.000	8847.3	0.630
7434.6	1.000	8886.7	0.616
7495.2	0.997	8926.1	0.603
7555.8	0.993	8965.5	0.591
7616.4	0.987	9005.0	0.578
7677.0	0.981	9044.4	0.562
7737.5	0.974	9083.8	0.545
7798.1	0.963	9123.2	0.528
7858.7	0.948	9162.7	0.509
7919.3	0.926	9202.1	0.488
7979.9	0.897	9241.5	0.465
8040.5	0.854	9280.9	0.442
8101.1	0.787	9320.3	0.413
8161.7	0.700	9359.8	0.378
8222.3	0.603	9399.2	0.341
8282.9	0.505	9438.6	0.301
8343.5	0.417	9478.0	0.261
8404.1	0.344	9517.5	0.222
8464.7	0.289	9556.9	0.186
8525.3	0.250	9596.3	0.157
8585.9	0.223	9635.7	0.135
8646.5	0.203	9675.2	0.118
8707.1	0.187	9714.6	0.102
8767.7	0.173	9754.0	0.087
8828.3	0.159	9793.4	0.073
8888.9	0.143	9832.9	0.062
8949.5	0.129	9872.3	0.051
9010.1	0.115	9911.7	0.040
9070.7	0.102	9951.1	0.029
9131.2	0.088	9990.6	0.021
9191.8	0.074	10030.0	0.015
9252.4	0.060	10069.4	0.011
9313.0	0.046	10108.8	0.007
9373.6	0.031	10148.3	0.005
9434.2	0.016	10187.7	0.002

TABLE 7

ENERGY RESPONSE FUNCTIONS, $S_x(\lambda)$, FOR GENEVA

U		*B1*		*B*		*B2*		*V1*		*V*		*G*	
λ (Å)	Trans	λ (Å)	Trans	λ (Å)	Trans	λ (Å)	Trans	λ (Å)	Trans	λ (Å)	Trans	λ (Å)	Trans
2909.4	0.000	3533.3	0.000	3580.5	0.000	4115.7	0.000	4972.4	0.000	4838.4	0.000	5498.3	0.000
2923.5	0.018	3550.3	0.001	3600.8	0.018	4125.1	0.004	4991.0	0.058	4864.2	0.023	5508.8	0.029
2937.6	0.036	3567.3	0.002	3621.2	0.036	4134.4	0.008	5009.6	0.116	4890.0	0.046	5519.4	0.059
2951.7	0.054	3584.4	0.003	3641.6	0.055	4143.8	0.012	5028.2	0.175	4915.7	0.071	5530.0	0.090
2965.9	0.072	3601.4	0.004	3661.9	0.076	4153.2	0.016	5046.8	0.233	4941.5	0.121	5540.5	0.123
2980.0	0.090	3618.5	0.006	3682.3	0.109	4162.5	0.020	5065.3	0.300	4967.3	0.213	5551.1	0.160
2994.1	0.108	3635.5	0.016	3702.6	0.157	4171.9	0.025	5083.9	0.389	4993.1	0.333	5561.6	0.211
3008.2	0.127	3652.6	0.038	3723.0	0.210	4181.2	0.032	5102.5	0.500	5018.9	0.457	5572.2	0.285
3022.4	0.148	3669.6	0.062	3743.4	0.264	4190.6	0.045	5121.1	0.613	5044.7	0.572	5582.7	0.377
3036.5	0.174	3686.7	0.087	3763.7	0.321	4200.0	0.064	5139.7	0.726	5070.5	0.666	5593.3	0.476
3050.6	0.203	3703.7	0.110	3784.1	0.383	4209.3	0.085	5158.2	0.832	5096.3	0.745	5603.8	0.580
3064.8	0.233	3720.8	0.139	3804.5	0.449	4218.7	0.105	5176.8	0.903	5122.1	0.824	5614.4	0.683

TABLE 7 (*Continued*)

U		*B1*		*B*		*B2*		*V1*		*V*		*G*	
λ (Å)	Trans	λ (Å)	Trans	λ (Å)	Trans	λ (Å)	Trans	λ (Å)	Trans	λ (Å)	Trans	λ (Å)	Trans
3078.9	0.262	3737.8	0.188	3824.8	0.517	4228.0	0.127	5195.4	0.934	5147.9	0.892	5625.0	0.770
3093.0	0.292	3754.8	0.257	3845.2	0.585	4237.4	0.148	5214.0	0.954	5173.7	0.933	5635.5	0.829
3107.1	0.321	3771.9	0.329	3865.6	0.647	4246.8	0.175	5232.5	0.974	5199.5	0.956	5646.1	0.869
3121.3	0.351	3788.9	0.399	3885.9	0.700	4256.1	0.216	5251.1	0.993	5225.2	0.977	5656.6	0.904
3135.4	0.381	3806.0	0.468	3906.3	0.745	4265.5	0.273	5269.7	0.999	5251.0	0.994	5667.2	0.938
3149.5	0.412	3823.0	0.536	3926.6	0.790	4274.9	0.332	5288.3	0.988	5276.8	1.000	5677.7	0.971
3163.7	0.443	3840.1	0.605	3947.0	0.835	4284.2	0.393	5306.9	0.969	5302.6	0.996	5688.3	0.993
3177.8	0.474	3857.1	0.674	3967.4	0.870	4293.6	0.455	5325.4	0.949	5328.4	0.992	5698.9	1.000
3191.9	0.506	3874.2	0.742	3987.7	0.896	4302.9	0.519	5344.0	0.929	5354.2	0.986	5709.4	0.995
3206.0	0.537	3891.2	0.809	4008.1	0.918	4312.3	0.581	5362.6	0.906	5380.0	0.973	5720.0	0.986
3220.2	0.569	3908.3	0.872	4028.5	0.940	4321.7	0.637	5381.2	0.878	5405.8	0.956	5730.5	0.976
3234.3	0.601	3925.3	0.920	4048.8	0.961	4331.0	0.685	5399.7	0.846	5431.6	0.938	5741.1	0.965
3248.4	0.632	3942.3	0.947	4069.2	0.974	4340.4	0.733	5418.3	0.813	5457.4	0.919	5751.6	0.950
3262.5	0.662	3959.4	0.961	4089.5	0.982	4349.7	0.781	5436.9	0.780	5483.2	0.897	5762.2	0.931
3276.7	0.690	3976.4	0.976	4109.9	0.990	4359.1	0.831	5455.5	0.747	5509.0	0.873	5772.7	0.909
3290.8	0.719	3993.5	0.989	4130.3	0.997	4368.5	0.882	5474.1	0.712	5534.7	0.848	5783.3	0.885
3304.9	0.748	4010.5	1.000	4150.6	1.000	4377.8	0.928	5492.6	0.676	5560.5	0.823	5793.9	0.860
3319.1	0.778	4027.6	0.990	4171.0	0.996	4387.2	0.955	5511.2	0.639	5586.3	0.796	5804.4	0.835
3333.2	0.807	4044.6	0.959	4191.4	0.989	4396.5	0.964	5529.8	0.602	5612.1	0.767	5815.0	0.809
3347.3	0.836	4061.7	0.923	4211.7	0.981	4405.9	0.973	5548.4	0.565	5637.9	0.738	5825.5	0.782
3361.4	0.864	4078.7	0.888	4232.1	0.972	4415.3	0.981	5567.0	0.529	5663.7	0.709	5836.1	0.755
3375.6	0.885	4095.8	0.853	4252.4	0.960	4424.6	0.989	5585.5	0.493	5689.5	0.679	5846.6	0.726
3389.7	0.901	4112.8	0.813	4272.8	0.944	4434.0	0.997	5604.1	0.458	5715.3	0.649	5857.2	0.697
3403.8	0.916	4129.8	0.758	4293.2	0.926	4443.4	1.000	5622.7	0.423	5741.1	0.618	5867.8	0.667
3417.9	0.932	4146.9	0.692	4313.5	0.908	4452.7	0.990	5641.3	0.388	5766.9	0.587	5878.3	0.638
3432.1	0.948	4163.9	0.625	4333.9	0.890	4462.1	0.971	5659.8	0.354	5792.7	0.555	5888.9	0.609
3446.2	0.964	4181.0	0.560	4354.3	0.871	4471.4	0.951	5678.4	0.323	5818.5	0.525	5899.4	0.579
3460.3	0.979	4198.0	0.495	4374.6	0.851	4480.8	0.931	5697.0	0.293	5844.2	0.494	5910.0	0.549
3474.5	0.994	4215.1	0.439	4395.0	0.832	4490.2	0.910	5715.6	0.263	5870.0	0.463	5920.5	0.517
3488.6	0.999	4232.1	0.393	4415.3	0.811	4499.5	0.888	5734.2	0.234	5895.8	0.433	5931.1	0.487
3502.7	0.997	4249.2	0.354	4435.7	0.791	4508.9	0.858	5752.7	0.206	5921.6	0.403	5941.6	0.458
3516.8	0.993	4266.2	0.316	4456.1	0.768	4518.2	0.818	5771.3	0.182	5947.4	0.375	5952.2	0.431
3531.0	0.989	4283.3	0.279	4476.4	0.745	4527.6	0.772	5789.9	0.162	5973.2	0.346	5962.8	0.404
3545.1	0.985	4300.3	0.242	4496.8	0.721	4537.0	0.725	5808.5	0.142	5999.0	0.318	5973.3	0.375
3559.2	0.980	4317.3	0.212	4517.2	0.696	4546.3	0.677	5827.1	0.123	6024.8	0.292	5983.9	0.347
3573.4	0.976	4334.4	0.187	4537.5	0.663	4555.7	0.627	5845.6	0.104	6050.6	0.267	5994.4	0.320
3587.5	0.972	4351.4	0.165	4557.9	0.622	4565.0	0.577	5864.2	0.088	6076.4	0.243	6005.0	0.296
3601.6	0.953	4368.5	0.143	4578.3	0.580	4574.4	0.529	5882.8	0.076	6102.2	0.219	6015.5	0.273
3615.7	0.918	4385.5	0.122	4598.6	0.537	4583.8	0.483	5901.4	0.066	6128.0	0.197	6026.1	0.249
3629.9	0.877	4402.6	0.102	4619.0	0.493	4593.1	0.435	5919.9	0.056	6153.7	0.177	6036.7	0.225
3644.0	0.836	4419.6	0.087	4639.3	0.447	4602.5	0.387	5938.5	0.046	6179.5	0.157	6047.2	0.202
3658.1	0.795	4436.7	0.076	4659.7	0.399	4611.9	0.338	5957.1	0.037	6205.3	0.138	6057.8	0.182
3672.2	0.754	4453.7	0.066	4680.1	0.351	4621.2	0.287	5975.7	0.031	6231.1	0.122	6068.3	0.164
3686.4	0.712	4470.8	0.055	4700.4	0.303	4630.6	0.243	5994.3	0.026	6256.9	0.107	6078.9	0.147
3700.5	0.670	4487.8	0.046	4720.8	0.262	4639.9	0.213	6012.8	0.021	6282.7	0.092	6089.4	0.129
3714.6	0.625	4504.9	0.037	4741.2	0.229	4649.3	0.190	6031.4	0.017	6308.5	0.078	6100.0	0.112
3728.8	0.573	4521.9	0.032	4761.5	0.199	4658.7	0.166	6050.0	0.013	6334.3	0.066	6110.5	0.097
3742.9	0.516	4538.9	0.027	4781.9	0.168	4668.0	0.141	6068.6	0.010	6360.1	0.057	6121.1	0.085
3757.0	0.460	4556.0	0.023	4802.2	0.139	4677.4	0.116	6087.2	0.008	6385.9	0.048	6131.7	0.074
3771.1	0.402	4573.0	0.019	4822.6	0.117	4686.7	0.093	6105.7	0.007	6411.7	0.039	6142.2	0.063
3785.3	0.345	4590.1	0.016	4843.0	0.100	4696.1	0.075	6124.3	0.005	6437.5	0.031	6152.8	0.053
3799.4	0.287	4607.1	0.013	4863.3	0.084	4705.5	0.065	6142.9	0.004	6463.2	0.026	6163.3	0.043
3813.5	0.230	4624.2	0.011	4883.7	0.068	4714.8	0.056	6161.5	0.003	6489.0	0.021	6173.9	0.035
3827.7	0.175	4641.2	0.010	4904.1	0.054	4724.2	0.046	6180.0	0.002	6514.8	0.016	6184.4	0.028
3841.8	0.137	4658.3	0.009	4924.4	0.044	4733.5	0.036	6198.6	0.002	6540.6	0.012	6195.0	0.022
3855.9	0.117	4675.3	0.008	4944.8	0.036	4742.9	0.026	6217.2	0.002	6566.4	0.009	6205.6	0.017
3870.0	0.100	4692.4	0.006	4965.1	0.027	4752.3	0.019	6235.8	0.001	6592.2	0.007	6216.1	0.011
3884.2	0.084	4709.4	0.005	4985.5	0.019	4761.6	0.015	6254.4	0.001	6618.0	0.004	6226.7	0.007
3898.3	0.067	4726.4	0.004	5005.9	0.014	4771.0	0.012	6272.9	0.001	6643.8	0.002	6237.2	0.005

TABLE 7 (*Continued*)

U		*B1*		*B*		*B2*		*V1*		*V*		*G*	
λ (Å)	Trans	λ (Å)	Trans	λ (Å)	Trans	λ (Å)	Trans	λ (Å)	Trans	λ (Å)	Trans	λ (Å)	Trans
3912.4	0.050	4743.5	0.003	5026.2	0.010	4780.4	0.009	6291.5	0.001	6669.6	0.001	6247.8	0.004
3926.5	0.034	4760.5	0.002	5046.6	0.007	4789.7	0.006	6310.1	0.000	6695.4	0.001	6258.3	0.002
3940.7	0.017	4777.6	0.001	5067.0	0.003	4799.1	0.003	6328.7	0.000	6721.2	0.000	6268.9	0.001

TABLE 8

ENERGY RESPONSE FUNCTIONS, $S_x(\lambda)$, FOR STROMGREN

u		*b*		*v*		*y*	
λ (Å)	Trans	λ (Å)	Trans	λ (Å)	Trans	λ (Å)	Trans
3162.5	0.000	4339.1	0.000	3737.4	0.000	5015.6	0.000
3171.4	0.008	4346.8	0.001	3748.3	0.002	5028.9	0.004
3180.2	0.017	4354.6	0.002	3759.3	0.004	5042.2	0.009
3189.1	0.029	4362.4	0.004	3770.3	0.006	5055.4	0.014
3198.0	0.045	4370.1	0.005	3781.3	0.009	5068.7	0.021
3206.8	0.063	4377.9	0.007	3792.3	0.011	5082.0	0.028
3215.7	0.084	4385.7	0.008	3803.2	0.014	5095.3	0.035
3224.6	0.109	4393.4	0.009	3814.2	0.018	5108.5	0.043
3233.4	0.138	4401.2	0.011	3825.2	0.022	5121.8	0.050
3242.3	0.174	4408.9	0.012	3836.2	0.026	5135.1	0.059
3251.2	0.218	4416.7	0.014	3847.2	0.031	5148.4	0.070
3260.0	0.264	4424.5	0.016	3858.2	0.037	5161.7	0.086
3268.9	0.315	4432.2	0.017	3869.1	0.044	5174.9	0.106
3277.8	0.368	4440.0	0.019	3880.1	0.052	5188.2	0.127
3286.6	0.422	4447.7	0.023	3891.1	0.061	5201.5	0.149
3295.5	0.476	4455.5	0.027	3902.1	0.071	5214.8	0.173
3304.4	0.530	4463.3	0.032	3913.1	0.085	5228.1	0.202
3313.2	0.585	4471.0	0.038	3924.0	0.102	5241.3	0.237
3322.1	0.640	4478.8	0.043	3935.0	0.124	5254.6	0.278
3331.0	0.692	4486.6	0.049	3946.0	0.150	5267.9	0.329
3339.8	0.737	4494.3	0.055	3957.0	0.181	5281.2	0.387
3348.7	0.776	4502.1	0.062	3968.0	0.220	5294.5	0.449
3357.6	0.811	4509.8	0.069	3979.0	0.267	5307.7	0.517
3366.4	0.843	4517.6	0.079	3989.9	0.324	5321.0	0.584
3375.3	0.873	4525.4	0.091	4000.9	0.390	5334.3	0.647
3384.2	0.899	4533.1	0.108	4011.9	0.464	5347.6	0.707
3393.0	0.922	4540.9	0.130	4022.9	0.543	5360.8	0.758
3401.9	0.942	4548.6	0.158	4033.9	0.625	5374.1	0.799
3410.8	0.958	4556.4	0.190	4044.8	0.707	5387.4	0.833
3419.7	0.971	4564.2	0.231	4055.8	0.782	5400.7	0.861
3428.5	0.982	4571.9	0.279	4066.8	0.845	5414.0	0.884
3437.4	0.988	4579.7	0.336	4077.8	0.898	5427.2	0.904
3446.3	0.991	4587.5	0.401	4088.8	0.938	5440.5	0.923
3455.1	0.994	4595.2	0.473	4099.8	0.968	5453.8	0.942
3464.0	0.997	4603.0	0.549	4110.7	0.988	5467.1	0.960
3472.9	1.000	4610.7	0.628	4121.7	0.998	5480.4	0.978
3481.7	0.999	4618.5	0.708	4132.7	0.997	5493.6	0.994

TABLE 8 (*Continued*)

u		*b*		*v*		*y*	
λ (Å)	Trans	λ (Å)	Trans	λ (Å)	Trans	λ (Å)	Trans
3490.6	0.994	4626.3	0.782	4143.7	0.982	5506.9	1.000
3499.5	0.987	4634.0	0.844	4154.7	0.950	5520.2	0.999
3508.3	0.981	4641.8	0.895	4165.6	0.903	5533.5	0.988
3517.2	0.974	4649.6	0.935	4176.6	0.842	5546.8	0.959
3526.1	0.967	4657.3	0.966	4187.6	0.767	5560.0	0.918
3534.9	0.961	4665.1	0.988	4198.6	0.685	5573.3	0.866
3543.8	0.953	4672.8	0.999	4209.6	0.600	5586.6	0.797
3552.7	0.941	4680.6	0.997	4220.6	0.516	5599.9	0.722
3561.5	0.920	4688.4	0.982	4231.5	0.441	5613.1	0.649
3570.4	0.893	4696.1	0.950	4242.5	0.377	5626.4	0.576
3579.3	0.867	4703.9	0.903	4253.5	0.323	5639.7	0.504
3588.1	0.840	4711.6	0.844	4264.5	0.276	5653.0	0.435
3597.0	0.812	4719.4	0.774	4275.5	0.235	5666.3	0.368
3605.9	0.780	4727.2	0.697	4286.4	0.199	5679.5	0.311
3614.7	0.743	4734.9	0.617	4297.4	0.167	5692.8	0.265
3623.6	0.706	4742.7	0.536	4308.4	0.138	5706.1	0.225
3632.5	0.669	4750.5	0.457	4319.4	0.116	5719.4	0.192
3641.3	0.631	4758.2	0.384	4330.4	0.098	5732.7	0.165
3650.2	0.589	4766.0	0.318	4341.4	0.084	5745.9	0.141
3659.1	0.543	4773.7	0.263	4352.3	0.071	5759.2	0.120
3667.9	0.495	4781.5	0.220	4363.3	0.061	5772.5	0.102
3676.8	0.447	4789.3	0.187	4374.3	0.052	5785.8	0.085
3685.7	0.397	4797.0	0.162	4385.3	0.047	5799.1	0.072
3694.6	0.350	4804.8	0.142	4396.3	0.043	5812.3	0.059
3703.4	0.306	4812.5	0.125	4407.2	0.040	5825.6	0.048
3712.3	0.265	4820.3	0.108	4418.2	0.037	5838.9	0.039
3721.2	0.228	4828.1	0.092	4429.2	0.034	5852.2	0.032
3730.0	0.195	4835.8	0.078	4440.2	0.031	5865.4	0.026
3738.9	0.165	4843.6	0.066	4451.2	0.029	5878.7	0.023
3747.8	0.134	4851.4	0.056	4462.2	0.026	5892.0	0.021
3756.6	0.104	4859.1	0.047	4473.1	0.022	5905.3	0.019
3765.5	0.075	4866.9	0.040	4484.1	0.018	5918.6	0.018
3774.4	0.054	4874.6	0.032	4495.1	0.015	5931.8	0.016
3783.2	0.041	4882.4	0.024	4506.1	0.011	5945.1	0.013
3792.1	0.031	4890.2	0.016	4517.1	0.009	5958.4	0.010
3801.0	0.021	4897.9	0.010	4528.1	0.006	5971.7	0.007
3809.8	0.010	4905.7	0.006	4539.0	0.003	5985.0	0.003

TABLE 9

ENERGY RESPONSE FUNCTIONS, $S_x(\lambda)$, FOR VILNIUS

U		*P*		*X*		*Y*		*Z*		*V*		*S*	
λ (Å)	Trans	λ (Å)	Trans	λ (Å)	Trans	λ (Å)	Trans	λ (Å)	Trans	λ (Å)	Trans	λ (Å)	Trans
3047.3	0.000	3533.8	0.000	3674.0	0.000	4346.0	0.000	4873.4	0.000	4985.5	0.000	5785.1	0.000
3057.6	0.002	3539.5	0.003	3686.7	0.005	4360.0	0.022	4882.0	0.001	5000.0	0.001	5809.5	0.004
3067.9	0.003	3545.1	0.006	3699.5	0.009	4373.9	0.044	4890.6	0.002	5014.5	0.002	5833.8	0.008

TABLE 9 (*Continued*)

U		*P*		*X*		*Y*		*Z*		*V*		*S*	
λ (Å)	Trans	λ (Å)	Trans	λ (Å)	Trans	λ (Å)	Trans	λ (Å)	Trans	λ (Å)	Trans	λ (Å)	Trans
3078.2	0.005	3550.8	0.009	3712.2	0.014	4387.9	0.067	4899.2	0.003	5029.0	0.003	5858.2	0.011
3088.4	0.008	3556.5	0.013	3725.0	0.020	4401.9	0.101	4907.8	0.004	5043.5	0.005	5882.5	0.016
3098.7	0.012	3562.1	0.016	3737.7	0.029	4415.9	0.157	4916.4	0.004	5058.0	0.009	5906.9	0.022
3109.0	0.018	3567.8	0.022	3750.5	0.039	4429.8	0.236	4925.0	0.005	5072.5	0.015	5931.3	0.030
3119.3	0.025	3573.5	0.030	3763.3	0.050	4443.8	0.325	4933.6	0.005	5087.0	0.021	5955.6	0.037
3129.5	0.032	3579.1	0.038	3776.0	0.063	4457.8	0.416	4942.2	0.006	5101.6	0.031	5980.0	0.043
3139.8	0.041	3584.8	0.047	3788.8	0.081	4471.8	0.505	4950.8	0.006	5116.1	0.047	6004.3	0.047
3150.1	0.052	3590.5	0.057	3801.5	0.104	4485.7	0.591	4959.4	0.007	5130.6	0.067	6028.7	0.049
3160.4	0.066	3596.1	0.068	3814.3	0.126	4499.7	0.676	4968.0	0.008	5145.1	0.088	6053.1	0.050
3170.6	0.080	3601.8	0.085	3827.0	0.152	4513.7	0.760	4976.6	0.008	5159.6	0.113	6077.4	0.050
3180.9	0.095	3607.4	0.107	3839.8	0.186	4527.7	0.835	4985.2	0.009	5174.1	0.143	6101.8	0.050
3191.2	0.113	3613.1	0.129	3852.6	0.226	4541.6	0.893	4993.8	0.010	5188.6	0.178	6126.1	0.049
3201.5	0.134	3618.8	0.152	3865.3	0.268	4555.6	0.929	5002.4	0.010	5203.1	0.214	6150.5	0.049
3211.7	0.157	3624.4	0.176	3878.1	0.312	4569.6	0.957	5011.0	0.010	5217.6	0.250	6174.9	0.049
3222.0	0.180	3630.1	0.204	3890.8	0.361	4583.6	0.982	5019.6	0.011	5232.1	0.287	6199.2	0.049
3232.3	0.205	3635.8	0.238	3903.6	0.415	4597.5	0.997	5028.2	0.012	5246.6	0.324	6223.6	0.052
3242.6	0.234	3641.4	0.274	3916.3	0.470	4611.5	0.998	5036.8	0.014	5261.1	0.362	6247.9	0.058
3252.8	0.264	3647.1	0.310	3929.1	0.526	4625.5	0.990	5045.4	0.017	5275.6	0.403	6272.3	0.068
3263.1	0.295	3652.8	0.348	3941.9	0.585	4639.5	0.978	5054.0	0.022	5290.1	0.453	6296.7	0.081
3273.4	0.327	3658.4	0.387	3954.6	0.646	4653.4	0.962	5062.6	0.029	5304.6	0.509	6321.0	0.095
3283.7	0.361	3664.1	0.429	3967.4	0.709	4667.4	0.939	5071.2	0.040	5319.1	0.567	6345.4	0.112
3293.9	0.396	3669.7	0.473	3980.1	0.771	4681.4	0.907	5079.8	0.059	5333.6	0.628	6369.7	0.142
3304.2	0.432	3675.4	0.519	3992.9	0.827	4695.3	0.871	5088.4	0.089	5348.1	0.697	6394.1	0.192
3314.5	0.470	3681.1	0.566	4005.6	0.876	4709.3	0.833	5097.0	0.130	5362.6	0.775	6418.5	0.272
3324.8	0.507	3686.7	0.613	4018.4	0.924	4723.3	0.795	5105.6	0.184	5377.1	0.855	6442.8	0.398
3335.0	0.545	3692.4	0.658	4031.2	0.969	4737.3	0.755	5114.2	0.258	5391.6	0.927	6467.2	0.610
3345.3	0.583	3698.1	0.700	4043.9	0.996	4751.2	0.714	5122.8	0.350	5406.1	0.968	6491.5	0.852
3355.6	0.623	3703.7	0.743	4056.7	0.999	4765.2	0.673	5131.4	0.450	5420.6	0.983	6515.9	0.992
3365.9	0.660	3709.4	0.785	4069.4	0.995	4779.2	0.631	5140.0	0.556	5435.2	0.993	6540.3	0.959
3376.1	0.695	3715.1	0.828	4082.2	0.990	4793.2	0.592	5148.6	0.667	5449.7	0.999	6564.6	0.779
3386.4	0.728	3720.7	0.867	4094.9	0.945	4807.1	0.554	5157.2	0.774	5464.2	0.988	6589.0	0.525
3396.7	0.762	3726.4	0.897	4107.7	0.859	4821.1	0.517	5165.8	0.864	5478.7	0.960	6613.3	0.339
3407.0	0.795	3732.0	0.921	4120.4	0.755	4835.1	0.480	5174.4	0.928	5493.2	0.928	6637.7	0.230
3417.2	0.825	3737.7	0.945	4133.2	0.650	4849.1	0.443	5183.0	0.974	5507.7	0.894	6662.1	0.155
3427.5	0.851	3743.4	0.969	4146.0	0.551	4863.0	0.409	5191.6	0.999	5522.2	0.856	6686.4	0.109
3437.8	0.878	3749.0	0.990	4158.7	0.461	4877.0	0.377	5200.2	0.994	5536.7	0.813	6710.8	0.082
3448.1	0.905	3754.7	0.999	4171.5	0.376	4891.0	0.345	5208.8	0.967	5551.2	0.768	6735.1	0.067
3458.3	0.929	3760.4	0.998	4184.2	0.290	4905.0	0.314	5217.4	0.923	5565.7	0.721	6759.5	0.056
3468.6	0.948	3766.0	0.995	4197.0	0.219	4918.9	0.286	5226.0	0.858	5580.2	0.675	6783.8	0.047
3478.9	0.966	3771.7	0.991	4209.7	0.178	4932.9	0.262	5234.6	0.778	5594.7	0.628	6808.2	0.042
3489.2	0.985	3777.4	0.984	4222.5	0.151	4946.9	0.241	5243.2	0.685	5609.2	0.580	6832.6	0.038
3499.4	0.997	3783.0	0.964	4235.3	0.124	4960.9	0.222	5251.8	0.581	5623.7	0.531	6856.9	0.035
3509.7	0.999	3788.7	0.926	4248.0	0.101	4974.8	0.203	5260.4	0.467	5638.2	0.484	6881.3	0.032
3520.0	0.996	3794.3	0.881	4260.8	0.086	4988.8	0.186	5269.0	0.356	5652.7	0.438	6905.6	0.028
3530.3	0.992	3800.0	0.836	4273.5	0.075	5002.8	0.172	5277.6	0.262	5667.2	0.393	6930.0	0.026
3540.5	0.985	3805.7	0.789	4286.3	0.065	5016.8	0.160	5286.2	0.186	5681.7	0.348	6954.4	0.025
3550.8	0.969	3811.3	0.736	4299.0	0.057	5030.7	0.148	5294.8	0.126	5696.2	0.301	6978.7	0.024
3561.1	0.946	3817.0	0.675	4311.8	0.052	5044.7	0.136	5303.4	0.082	5710.7	0.253	7003.1	0.023
3571.4	0.921	3822.7	0.609	4324.6	0.051	5058.7	0.126	5312.0	0.056	5725.2	0.203	7027.4	0.021
3581.6	0.894	3828.3	0.541	4337.3	0.050	5072.7	0.116	5320.6	0.041	5739.7	0.153	7051.8	0.020
3591.9	0.856	3834.0	0.473	4350.1	0.050	5086.6	0.107	5329.2	0.032	5754.2	0.111	7076.2	0.019
3602.2	0.807	3839.7	0.408	4362.8	0.053	5100.6	0.098	5337.8	0.026	5768.8	0.083	7100.5	0.019
3612.5	0.753	3845.3	0.351	4375.6	0.058	5114.6	0.090	5346.4	0.023	5783.3	0.065	7124.9	0.019
3622.7	0.697	3851.0	0.298	4388.3	0.064	5128.6	0.084	5355.0	0.023	5797.8	0.048	7149.2	0.018
3633.0	0.636	3856.7	0.244	4401.1	0.070	5142.5	0.078	5363.6	0.026	5812.3	0.034	7173.6	0.018
3643.3	0.569	3862.3	0.189	4413.9	0.076	5156.5	0.074	5372.2	0.031	5826.8	0.026	7198.0	0.016
3653.6	0.497	3868.0	0.142	4426.6	0.083	5170.5	0.069	5380.8	0.037	5841.3	0.024	7222.3	0.015
3663.8	0.423	3873.6	0.111	4439.4	0.090	5184.5	0.064	5389.4	0.043	5855.8	0.023	7246.7	0.015
3674.1	0.354	3879.3	0.092	4452.1	0.097	5198.4	0.059	5398.0	0.048	5870.3	0.021	7271.0	0.014

TABLE 9 (*Continued*)

U		*P*		*X*		*Y*		*Z*		*V*		*S*	
λ (Å)	Trans	λ (Å)	Trans	λ (Å)	Trans	λ (Å)	Trans	λ (Å)	Trans	λ (Å)	Trans	λ (Å)	Trans
3684.4	0.296	3885.0	0.073	4464.9	0.098	5212.4	0.054	5406.6	0.052	5884.8	0.020	7295.4	0.013
3694.7	0.247	3890.6	0.054	4477.6	0.092	5226.4	0.049	5415.2	0.053	5899.3	0.019	7319.8	0.012
3704.9	0.197	3896.3	0.038	4490.4	0.085	5240.4	0.045	5423.8	0.052	5913.8	0.017	7344.1	0.012
3715.2	0.150	3902.0	0.028	4503.2	0.077	5254.3	0.040	5432.4	0.049	5928.3	0.016	7368.5	0.011
3725.5	0.113	3907.6	0.024	4515.9	0.069	5268.3	0.036	5441.0	0.046	5942.8	0.015	7392.8	0.009
3735.8	0.089	3913.3	0.020	4528.7	0.062	5282.3	0.031	5449.6	0.042	5957.3	0.013	7417.2	0.008
3746.0	0.067	3919.0	0.016	4541.4	0.053	5296.3	0.027	5458.2	0.037	5971.8	0.011	7441.6	0.007
3756.3	0.044	3924.6	0.012	4554.2	0.045	5310.2	0.023	5466.8	0.031	5986.3	0.010	7465.9	0.006
3766.6	0.028	3930.3	0.009	4566.9	0.036	5324.2	0.018	5475.4	0.026	6000.8	0.008	7490.3	0.006
3776.9	0.019	3935.9	0.007	4579.7	0.028	5338.2	0.014	5484.0	0.020	6015.3	0.006	7514.6	0.005
3787.1	0.013	3941.6	0.004	4592.5	0.019	5352.1	0.009	5492.6	0.013	6029.8	0.004	7539.0	0.003
3797.4	0.006	3947.3	0.002	4605.2	0.009	5366.1	0.005	5501.2	0.007	6044.3	0.002	7563.4	0.001

TABLE 10

ENERGY RESPONSE FUNCTIONS, $S_x(\lambda)$, FOR WBVR

W		*B*		*V*		*R*	
λ (Å)	Trans	λ (Å)	Trans	λ (Å)	Trans	λ (Å)	Trans
2908.2	0.000	3486.0	0.000	4619.9	0.000	6039.9	0.000
2923.2	0.000	3510.9	0.000	4650.4	0.001	6084.0	0.000
2938.3	0.000	3535.8	0.000	4680.9	0.002	6128.1	0.002
2953.3	0.001	3560.6	0.000	4711.4	0.004	6172.2	0.008
2968.4	0.001	3585.5	0.001	4741.9	0.011	6216.3	0.037
2983.4	0.002	3610.4	0.005	4772.4	0.023	6260.4	0.102
2998.5	0.004	3635.2	0.013	4802.9	0.043	6304.4	0.222
3013.5	0.006	3660.1	0.030	4833.4	0.079	6348.5	0.389
3028.6	0.009	3685.0	0.054	4863.9	0.131	6392.6	0.570
3043.6	0.013	3709.9	0.085	4894.3	0.199	6436.7	0.733
3058.7	0.019	3734.7	0.121	4924.8	0.282	6480.8	0.856
3073.7	0.025	3759.6	0.158	4955.3	0.375	6524.9	0.939
3088.8	0.034	3784.5	0.196	4985.8	0.471	6569.0	0.983
3103.8	0.044	3809.3	0.234	5016.3	0.562	6613.1	0.998
3118.9	0.055	3834.2	0.273	5046.8	0.645	6657.2	0.995
3133.9	0.068	3859.1	0.311	5077.3	0.716	6701.3	0.980
3149.0	0.083	3884.0	0.349	5107.8	0.777	6745.4	0.959
3164.0	0.099	3908.8	0.389	5138.3	0.830	6789.5	0.933
3179.1	0.116	3933.7	0.428	5168.7	0.874	6833.6	0.906
3194.1	0.133	3958.6	0.466	5199.2	0.910	6877.7	0.881
3209.2	0.152	3983.4	0.502	5229.7	0.940	6921.8	0.856
3224.2	0.171	4008.3	0.538	5260.2	0.963	6965.9	0.829
3239.2	0.192	4033.2	0.573	5290.7	0.980	7010.0	0.802
3254.3	0.213	4058.1	0.608	5321.2	0.991	7054.1	0.774
3269.3	0.236	4082.9	0.643	5351.7	0.998	7098.2	0.747
3284.4	0.259	4107.8	0.677	5382.2	1.000	7142.3	0.721
3299.4	0.283	4132.7	0.709	5412.7	0.997	7186.4	0.695
3314.5	0.308	4157.5	0.739	5443.1	0.990	7230.5	0.667
3329.5	0.334	4182.4	0.767	5473.6	0.981	7274.6	0.641
3344.6	0.360	4207.3	0.793	5504.1	0.969	7318.7	0.616
3359.6	0.388	4232.2	0.817	5534.6	0.953	7362.8	0.592
3374.7	0.416	4257.0	0.841	5565.1	0.936	7406.9	0.570
3389.7	0.447	4281.9	0.863	5595.6	0.915	7450.9	0.548
3404.8	0.480	4306.8	0.885	5626.1	0.889	7495.0	0.526
3419.8	0.515	4331.6	0.906	5656.6	0.859	7539.1	0.504
3434.9	0.553	4356.5	0.928	5687.1	0.828	7583.2	0.484
3449.9	0.593	4381.4	0.948	5717.5	0.796	7627.3	0.466

TABLE 10 (*Continued*)

W		*B*		*V*		*R*	
λ (Å)	Trans	λ (Å)	Trans	λ (Å)	Trans	λ (Å)	Trans
3465.0	0.637	4406.3	0.967	5748.0	0.761	7671.4	0.446
3480.0	0.680	4431.1	0.982	5778.5	0.724	7715.5	0.424
3495.1	0.723	4456.0	0.994	5809.0	0.683	7759.6	0.404
3510.1	0.763	4480.9	1.000	5839.5	0.640	7803.7	0.386
3525.2	0.803	4505.7	0.998	5870.0	0.597	7847.8	0.368
3540.2	0.842	4530.6	0.989	5900.5	0.550	7891.9	0.349
3555.3	0.878	4555.5	0.971	5931.0	0.503	7936.0	0.332
3570.3	0.912	4580.4	0.941	5961.5	0.457	7980.1	0.315
3585.4	0.943	4605.2	0.902	5992.0	0.417	8024.2	0.298
3600.4	0.968	4630.1	0.854	6022.4	0.381	8068.3	0.281
3615.5	0.985	4655.0	0.799	6052.9	0.348	8112.4	0.265
3630.5	0.997	4679.8	0.741	6083.4	0.316	8156.5	0.249
3645.6	0.999	4704.7	0.680	6113.9	0.287	8200.6	0.233
3660.6	0.986	4729.6	0.617	6144.4	0.259	8244.7	0.217
3675.6	0.962	4754.4	0.555	6174.9	0.232	8288.8	0.202
3690.7	0.927	4779.3	0.494	6205.4	0.205	8332.9	0.186
3705.7	0.873	4804.2	0.438	6235.9	0.180	8377.0	0.170
3720.8	0.801	4829.1	0.387	6266.4	0.156	8421.1	0.155
3735.8	0.716	4853.9	0.340	6296.8	0.135	8465.2	0.140
3750.9	0.625	4878.8	0.297	6327.3	0.116	8509.3	0.126
3765.9	0.532	4903.7	0.257	6357.8	0.099	8553.3	0.112
3781.0	0.437	4928.5	0.217	6388.3	0.084	8597.4	0.098
3796.0	0.343	4953.4	0.180	6418.8	0.071	8641.5	0.085
3811.1	0.260	4978.3	0.145	6449.3	0.060	8685.6	0.072
3826.1	0.193	5003.2	0.115	6479.8	0.050	8729.7	0.060
3841.2	0.135	5028.0	0.090	6510.3	0.041	8773.8	0.049
3856.2	0.086	5052.9	0.069	6540.8	0.034	8817.9	0.039
3871.3	0.051	5077.8	0.051	6571.2	0.027	8862.0	0.030
3886.3	0.031	5102.6	0.037	6601.7	0.022	8906.1	0.023
3901.4	0.017	5127.5	0.026	6632.2	0.018	8950.2	0.017
3916.4	0.007	5152.4	0.017	6662.7	0.014	8994.3	0.012
3931.5	0.002	5177.3	0.010	6693.2	0.012	9038.4	0.009
3946.5	0.001	5202.1	0.006	6723.7	0.009	9082.5	0.006
3961.6	0.000	5227.0	0.003	6754.2	0.007	9126.6	0.005
3976.6	0.000	5251.9	0.002	6784.7	0.006	9170.7	0.003
3991.7	0.000	5276.7	0.001	6815.2	0.006	9214.8	0.002
4006.7	0.000	5301.6	0.000	6845.6	0.004	9258.9	0.001

TABLE 11
ENERGY RESPONSE FUNCTIONS, $S_x(\lambda)$, FOR COUSINS

R		I	
λ (Å)	Trans	λ (Å)	Trans
5507.0	0.000	7028.9	0.000
5553.0	0.106	7058.8	0.025
5598.9	0.241	7088.7	0.051
5644.8	0.431	7118.6	0.083
5690.7	0.631	7148.5	0.138
5736.6	0.769	7178.4	0.210
5782.5	0.853	7208.3	0.285
5828.4	0.910	7238.2	0.366
5874.4	0.948	7268.1	0.452
5920.3	0.975	7297.9	0.540
5966.2	0.989	7327.8	0.621
6012.1	0.997	7357.7	0.691
6058.0	1.000	7387.6	0.754
6103.9	0.999	7417.5	0.812
6149.9	0.997	7447.4	0.858
6195.8	0.992	7477.3	0.890
6241.7	0.986	7507.2	0.919
6287.6	0.979	7537.1	0.944
6333.5	0.970	7567.0	0.962
6379.4	0.960	7596.9	0.976
6425.3	0.948	7626.7	0.989
6471.3	0.934	7656.6	0.995
6517.2	0.918	7686.5	0.998
6563.1	0.900	7716.4	0.999
6609.0	0.884	7746.3	1.000
6654.9	0.867	7776.2	0.999
6700.8	0.849	7806.1	0.998
6746.7	0.828	7836.0	0.997
6792.7	0.805	7865.9	0.996
6838.6	0.780	7895.8	0.995
6884.5	0.755	7925.7	0.995
6930.4	0.730	7955.6	0.995
6976.3	0.704	7985.4	0.997
7022.2	0.678	8015.3	0.998
7068.2	0.652	8045.2	0.999
7114.1	0.626	8075.1	0.998
7160.0	0.601	8105.0	0.997
7205.9	0.576	8134.9	0.995
7251.8	0.549	8164.8	0.990
7297.7	0.521	8194.7	0.985
7343.6	0.492	8224.6	0.979
7389.6	0.463	8254.5	0.974
7435.5	0.434	8284.4	0.967
7481.4	0.407	8314.3	0.961
7527.3	0.379	8344.1	0.952
7573.2	0.352	8374.0	0.942
7619.1	0.325	8403.9	0.930
7665.0	0.299	8433.8	0.918
7711.0	0.274	8463.7	0.905
7756.9	0.251	8493.6	0.892
7802.8	0.229	8523.5	0.877
7848.7	0.208	8553.4	0.859
7894.6	0.188	8583.3	0.837
7940.5	0.167	8613.2	0.815
7986.4	0.148	8643.1	0.784
8032.4	0.130	8673.0	0.743
8078.3	0.114	8702.8	0.698
8124.2	0.101	8732.7	0.649

TABLE 11 (*Continued*)

R		I	
λ (Å)	Trans	λ (Å)	Trans
8170.1	0.090	8762.6	0.593
8216.0	0.080	8792.5	0.530
8261.9	0.071	8822.4	0.467
8307.9	0.063	8852.3	0.404
8353.8	0.055	8882.2	0.343
8399.7	0.047	8912.1	0.282
8445.6	0.040	8942.0	0.226
8491.5	0.033	8971.9	0.178
8537.4	0.027	9001.8	0.134
8583.3	0.021	9031.7	0.094
8629.3	0.017	9061.5	0.064
8675.2	0.014	9091.4	0.043
8721.1	0.012	9121.3	0.024
8767.0	0.009	9151.2	0.010
8812.9	0.006	9181.1	0.005
8858.8	0.003	9211.0	0.003

TABLE 12
ENERGY RESPONSE FUNCTIONS, $S_x(\lambda)$, FOR TYCHO

Bt		Vt	
λ (Å)	Trans	λ (Å)	Trans
3511.4	0.000	4494.7	0.000
3532.8	0.007	4525.9	0.014
3554.2	0.015	4557.2	0.042
3575.5	0.029	4588.5	0.094
3596.9	0.050	4619.7	0.175
3618.3	0.074	4651.0	0.280
3639.7	0.102	4682.3	0.399
3661.1	0.134	4713.6	0.523
3682.5	0.169	4744.8	0.638
3703.9	0.208	4776.1	0.734
3725.3	0.249	4807.4	0.807
3746.7	0.292	4838.6	0.863
3768.1	0.338	4869.9	0.901
3789.4	0.387	4901.2	0.930
3810.8	0.436	4932.4	0.953
3832.2	0.486	4963.7	0.970
3853.6	0.536	4995.0	0.983
3875.0	0.584	5026.3	0.993
3896.4	0.630	5057.5	0.998
3917.8	0.673	5088.8	1.000
3939.2	0.713	5120.1	0.998
3960.6	0.748	5151.3	0.992
3982.0	0.779	5182.6	0.982
4003.3	0.806	5213.9	0.970
4024.7	0.828	5245.2	0.955
4046.1	0.846	5276.4	0.938
4067.5	0.862	5307.7	0.920
4088.9	0.874	5339.0	0.901
4110.3	0.885	5370.2	0.881
4131.7	0.896	5401.5	0.859
4153.1	0.905	5432.8	0.837
4174.5	0.915	5464.0	0.813

TABLE 12 (*Continued*)

Bt		Vt	
λ (Å)	Trans	λ (Å)	Trans
4195.9	0.926	5495.3	0.789
4217.2	0.937	5526.6	0.764
4238.6	0.948	5557.9	0.739
4260.0	0.959	5589.1	0.713
4281.4	0.970	5620.4	0.687
4302.8	0.980	5651.7	0.659
4324.2	0.989	5682.9	0.631
4345.6	0.996	5714.2	0.602
4367.0	1.000	5745.5	0.573
4388.4	0.996	5776.8	0.544
4409.8	0.983	5808.0	0.515
4431.2	0.957	5839.3	0.486
4452.5	0.916	5870.6	0.457
4473.9	0.862	5901.8	0.427
4495.3	0.797	5933.1	0.398
4516.7	0.724	5964.4	0.370
4538.1	0.645	5995.7	0.343
4559.5	0.565	6026.9	0.317
4580.9	0.485	6058.2	0.291
4602.3	0.411	6089.5	0.267
4623.7	0.343	6120.7	0.245
4645.1	0.283	6152.0	0.225
4666.4	0.236	6183.3	0.207
4687.8	0.195	6214.5	0.189
4709.2	0.164	6245.8	0.172
4730.6	0.139	6277.1	0.157
4752.0	0.120	6308.4	0.143
4773.4	0.105	6339.6	0.131
4794.8	0.094	6370.9	0.120
4816.2	0.085	6402.2	0.110
4837.6	0.076	6433.4	0.100
4859.0	0.068	6464.7	0.091
4880.3	0.059	6496.0	0.082
4901.7	0.050	6527.3	0.073
4923.1	0.042	6558.5	0.065
4944.5	0.033	6589.8	0.058
4965.9	0.025	6621.1	0.050
4987.3	0.017	6652.3	0.042
5008.7	0.011	6683.6	0.033
5030.1	0.006	6714.9	0.024
5051.5	0.003	6746.2	0.016
5072.9	0.001	6777.4	0.008

TABLE 13

ENERGY RESPONSE FUNCTIONS, $S_x(\lambda)$, FOR HIPPARCOS

Hp	
λ (Å)	Trans
3460.5	0.000
3540.3	0.032
3620.1	0.061
3699.9	0.097
3779.6	0.143
3859.4	0.193

TABLE 13 (*Continued*)

Hp	
λ (Å)	Trans
3939.2	0.244
4018.9	0.301
4098.7	0.362
4178.5	0.423
4258.2	0.487
4338.0	0.558
4417.8	0.639
4497.5	0.719
4577.3	0.792
4657.1	0.858
4736.8	0.918
4816.6	0.961
4896.4	0.986
4976.1	0.998
5055.9	0.999
5135.7	0.993
5215.4	0.981
5295.2	0.964
5375.0	0.940
5454.7	0.913
5534.5	0.885
5614.3	0.856
5694.0	0.825
5773.8	0.792
5853.6	0.760
5933.3	0.728
6013.1	0.695
6092.9	0.662
6172.6	0.630
6252.4	0.598
6332.2	0.566
6411.9	0.536
6491.7	0.506
6571.5	0.478
6651.2	0.450
6731.0	0.423
6810.8	0.397
6890.5	0.371
6970.3	0.347
7050.1	0.322
7129.8	0.299
7209.6	0.275
7289.4	0.252
7369.2	0.229
7448.9	0.209
7528.7	0.189
7608.5	0.171
7688.2	0.153
7768.0	0.137
7847.8	0.122
7927.5	0.109
8007.3	0.097
8087.1	0.086
8166.8	0.076
8246.6	0.067
8326.4	0.058
8406.1	0.048
8485.9	0.040
8565.7	0.033

TABLE 13 (*Continued*)

Hp	
λ (Å)	Trans
8645.4	0.027
8725.2	0.022
8805.0	0.018
8884.7	0.015
8964.5	0.012

TABLE 13 (*Continued*)

Hp	
λ (Å)	Trans
9044.3	0.009
9124.0	0.006
9203.8	0.004
9283.6	0.002

REFERENCES

Abazajian, K. N., Adelman-McCarthy, J. K., Agüeros, M. A., et al. 2009, ApJS, 182, 543

Allard, F., Homeier, D., Freytag, B., & Sharp, C. M. 2012, in EAS Publications Series 57, 3

Arp, H. C. 1958, AJ, 63, 118

Berger, D. H., Gies, D. R., McAlister, H. A., et al. 2006, ApJ, 644, 475

Bessell, M. S. 1990, PASP, 102, 1181

———. 2011, PASP, 123, 1442

Bessell, M. S., & Brett, J. M. 1988, PASP , 100, 1134

Bessell, M., & Murphy, S. 2012, PASP, 124, 140

Blackwell, D. E., & Shallis, M. J. 1977, MNRAS, 180, 177

Bohlin, R. C., Dickinson, M. E., & Calzetti, D. 2001, AJ , 122, 2118

Bohlin, R. C., & Gilliland, R. L. 2004a, AJ, 128, 3053

———. 2004b, AJ, 127, 3508

Bohlin, R. C., Gordon, K. D., & Tremblay, P.-E. 2014, PASP, 126, 711

Boyajian, T. S., von Braun, K., van Belle, G., et al. 2012, ApJ, 757, 112

———. 2013, ApJ, 771, 40

Casagrande, L., Portinari, L., & Flynn, C. 2006, MNRAS, 373, 13

Casagrande, L., Ramírez, I., Meléndez, J., Bessell, M., & Asplund, M. 2010, A&A, 512, A 54

Casagrande, L., & VandenBerg, D. A. 2014, MNRAS, 444, 392

Chen, Y., Trager, S., Peletier, R., & Lançon, A. 2011, J. Phys. Conf. Ser., 328, 012023

Cohen, M., Walker, R. G., Barlow, M. J., & Deacon, J. R. 1992, AJ, 104, 1650

Cohen, M., Wheaton, W. A., & Megeath, S. T. 2003, AJ, 126, 1090

Cousins, A. W. J. 1976, MmRAS, 81, 25

Crawford, D. L., & Mander, J. 1966, AJ, 71, 114

Cushing, M. C., Rayner, J. T., & Vacca, W. D. 2005, ApJ, 623, 1115

Cushing, M. C., Vacca, W. D., & Rayner, J. T. 2004, PASP, 116, 362

Eggen, O. J. 1965, AJ, 70, 19

Falcón-Barroso, J., Sánchez-Blázquez, P., Vazdekis, A., et al. 2011, A&A, 532, A 95

Gaidos, E., Mann, A. W., Lépine, S., et al. 2014, MNRAS, 443, 2561

Golay, M. 1972, Vistas Astron., 14, 13

Gregg, M. D., Silva, D., Rayner, J., et al. 2006, in The 2005 *HST* Calibration Workshop: Hubble After the Transition to Two-Gyro Mode, ed. A. M. Koekemoer, P. Goudfrooij, & L. L. Dressel, (Greenbelt: GSFC), 209

Häggkvist, L., & Oja, T. 1970, A&AS, 1, 199

Heap, S. R., & Lindler, D. J. 2007, in ASP Conf. Ser. 374, From Stars to Galaxies: Building the Pieces to Build Up the Universe, ed. A. Vallenari, R. Tantalo, L. Portinari, & A. Moretti (San Francisco: ASP), 409

Høg, E., Fabricius, C., Makarov, V. V., et al. 2000, A&A, 355, L 27

Huber, D., Chaplin, W. J., Christensen-Dalsgaard, J., et al. 2013, ApJ, 767, 127

Ireland, M. J., Mérand, A., ten Brummelaar, T. A., et al. 2008, Proc. SPIE, 7013

Johnson, H. L., & Morgan, W. W. 1951, ApJ, 114, 522

Jones, D. H. P., Sinclair, J. E., & Alexander, J. B. 1981, MNRAS, 194, 403

Kakaras, G., Straizys, V., Sudzius, J., & Zdanavicius, K. 1968, Vilnius Astronomijos Observatorijos Biuletenis, 22, 3

Kornilov, V. G., Volkov, I. M., Zakharov, A. I., et al. 1991, Trudy Gosudarstvennogo Astronomicheskogo Instituta, 63, 1

Maíz Apellániz, J. 2006, AJ, 131, 1184

Mamajek, E. E., Meyer, M. R., & Liebert, J. 2002, AJ, 124, 1670

Mann, A. W., Brewer, J. M., Gaidos, E., Lépine, S., & Hilton, E. J. 2013a, AJ, 145, 52

Mann, A. W., Gaidos, E., & Aldering, G. 2011, PASP, 123, 1273

Mann, A. W., Gaidos, E., & Ansdell, M. 2013b, ApJ, 779, 188

McClure, R. D. 1976, AJ, 81, 182

Mendoza v, E. E. 1963, Boletin de los Observatorios Tonantzintla y Tacubaya, 3, 137

Mermilliod, J.-C., Mermilliod, M., & Hauck, B. 1997, A&AS, 124, 349

Pickles, A. J. 1998, PASP, 110, 863

Rayner, J. T., Cushing, M. C., & Vacca, W. D. 2009, ApJS, 185, 289

Samus, N. N., Durlevich, O. V., et al. 2004, VizieR Online Data Catalog , 2250, 0

Samus, N. N., Kazarovets, E. V., Kireeva, N. N., Pastukhova, E. N., & Durlevich, O. V. 2010, Odessa Astronomical Publications, 23, 102

Sánchez-Blázquez, P., Gorgas, J., Cardiel, N., & González, J. J. 2006, A&A, 457, 787

Skrutskie, M. F., Cutri, R. M., Stiening, R., et al. 2006, AJ, 131, 1163

Sneden, C. A. 1973, PhD thesis, the University of Texas at Austin

Sousa, S. G., Alapini, A., Israelian, G., & Santos, N. C. 2010, A&A, 512, A 13

Sousa, S. G., Santos, N. C., Israelian, G., Mayor, M., & Udry, S. 2011, A&A, 533, A 141

Spearman, C. 1904, Am. J. Psych., 15, 88

Stoughton, C., Lupton, R. H., Bernardi, M., et al. 2002, AJ, 123, 485

Straizys, V. 1996, Baltic Astron., 5, 459

Strömgren, B. 1956, Vistas Astron., 2, 1336
ten Brummelaar, T. A., Sturmann, L., Sturmann, J., et al. 2012, Proc. SPIE, 8447
Vacca, W. D., Cushing, M. C., & Rayner, J. T. 2003, PASP, 115, 389
Valdes, F., Gupta, R., Rose, J. A., Singh, H. P., & Bell, D. J. 2004, ApJS, 152, 251
Valenti, J. A., & Piskunov, N. 1996, A&AS, 118, 595
van Belle, G. T., van Belle, G., Creech- Eakman, M. J., et al. 2008, ApJS, 176, 276
van Leeuwen, F. 2007, A&A, 474, 653
van Leeuwen, F., & Fantino, E. 2005, A&A, 439, 791
von Braun, K., Boyajian, T. S., van Belle, G. T., et al. 2014, MNRAS, 438, 2413
Young, A. T., Genet, R. M., Boyd, L. J., et al. 1991, PASP, 103, 221